Residual Stress in Engineering Materials: A Review

Ali Tabatabaeian [a*], Ahmad Reza Ghasemi [b*], Mahmood M. Shokrieh [c], Bahareh Marzbanrad [d], Mohammad Baraheni [b, e], Mohammad Fotouhi [a]

[a] *James Watt School of Engineering, University of Glasgow, Glasgow, UK.*

[b] *Composite and Nanocomposite Research Laboratory, Department of Solid Mechanics, Faculty of Mechanical Engineering, University of Kashan, Kashan, Iran.*

[c] *Composite Research Laboratory, Center of Excellence in Experimental Solid Mechanics and Dynamics, School of Mechanical Engineering, Iran University of Science and Technology, Tehran, Iran.*

[d] *Mechanical and Mechatronics Engineering Department, University of Waterloo, Canada.*

[e] *Institute of Precision Machining, Hochschule Furtwangen University, Villingen, Germany.*

[*]Corresponding authors:

2611578T@student.gla.ac.uk (A. Tabatabaeian)

ghasemi@kashanu.ac.ir (Dr. A.R. Ghasemi)

Abstract

The accurate determination of residual stresses has a crucial role in understanding the complex interactions between microstructure, mechanical state, mode(s) of failure, and structural integrity. Moreover, the residual stress management concept contributes to industrial applications aiming to improve the product's service performance and life cycle. In this regard, the industry requests rapid, efficient, and modern methods to identify and control the residual stress state. This review paper contains three main sections. The first section covers different residual stress determination methods and reports the advancements over the recent decade. The second section includes the role of residual stresses in the performance of a broad range of materials including metallic alloys, polymers, ceramics, composites, and biomaterials. This is presented by classifying different science areas dealing with residual stresses into two main groups, including ‘origins’ and ‘effects’ of residual stresses. The range of topics covered are “welding, machining, curing/cooling, and spray coating processes”, “medical and dental sciences”, and “fatigue and fracture mechanisms”. The third section summarizes various strategies to effectively control residual stresses through

different manufacturing procedures. It is hoped that the data provided in this review will serve as a valuable up-to-date reference for engineers and scientists in the field of residual stress.

Keywords: Residual stress, Experimental & analytical methods, Curing and cooling, Spray coating, Machining & welding processes, Fatigue & fracture.

1. Introduction

Residual stresses, also known as trapped or locked stresses, are self-balanced and non-homogenous stresses generated during different manufacturing processes of engineering components. A unique feature of these non-linear stresses is their presence in the lack of external mechanical or thermal loads in solid materials. In other words, these are specific stresses which remain within a material after the manufacturing stage, when there is neither external force nor thermal gradient [1]–[3]. This underscores that residual stresses are entirely different from normal stresses that arise from processes in which forces are generated on a fixed boundary condition [4]–[6].

When it comes to causes of residual stresses, two prime types of materials must be taken into account including ‘metallic alloys and ceramics’ [7] and ‘polymers and composites’ [8]. In the former, residual stresses are mainly generated through the surface layer due to machining, welding, heat treatment, etc. In contrast, in composites, orthotropic behavior because of different layer directions, as well as a mismatch in thermo-mechanical properties of dissimilar layers, particularly coefficient of thermal expansion (CTE), results in the creation of residual stresses during the cooling or curing processes. In either of the mentioned groups, three levels of stress are often defined as presented here:

a) Metallic and ceramic structures:

Type-1: Macro residual stresses generated on a scale larger than the grain size of the material during the manufacturing procedure.

Type-2: Micro residual stresses, which vary on the scale of individual grain caused by the manufacturing procedure.

Type-3: Micro residual stresses caused by crystalline defects within a grain.

b) Polymeric composite structures:

Type-1: Structural scale residual stresses due to variation in shrinkage through the laminate thickness.

Type-2: Macro residual stresses forming in ply-to-ply scale resulting from the anisotropic difference in CTE.

Type-3: Micro residual stresses created between matrix and fiber phases within each ply due to different thermo-mechanical properties.

A wealth of research has established that residual stresses can alter different engineering systems' mechanical and functional performances [9]–[11]. This is because when residual stresses are created in structures, a part of their strength is spent to overcome these stresses trapped inside them, resulting in catastrophic failure to occur sooner than expected. In addition to fatigue life, dimensional stability, corrosion resistance, distortion, matrix crack delamination, and warpage can be highly influenced by the presence of residual stresses [12][13]. On a broader look, residual stress plays a vital role in the function of bio-systems such as blood vessels [14]. One can take advantage of these stresses, purposely causing compressive residual stresses into the surface layer of components to improve fatigue life. Accordingly, these stresses can bring both detrimental and beneficial effects, and their quantification and analysis are of great importance across many sectors [15].

Despite the numerous studies that have been performed on the residual stress analysis in engineering materials, there is no review paper regarding classifying, comparing, and analyzing outcomes of recently published research and thoroughly investigating the progress, challenges and future perspectives in this field. In this regard, this paper represents a comprehensive review, including a close inspection of research throughout the recent decade. The focus here is on the research papers published from 2010 to 2020. However, a limited number of significant works before 2010 are reviewed in some sections. A study of nearly 300 research papers highlights that ‘various determination methods’, ‘different cutting-edge procedures associated with residual stresses’ and ‘methods to control or reduce residual stresses’ are the most critical areas that should be covered. This review is presented in three main sections, namely “determination methods”, “origins and effects”, and “control methods”, aiming at responding to three critical questions (Fig.

1). Finally, a summary of the reported subjects and the outlooks for future works will be discussed in the “conclusions and perspectives” part.

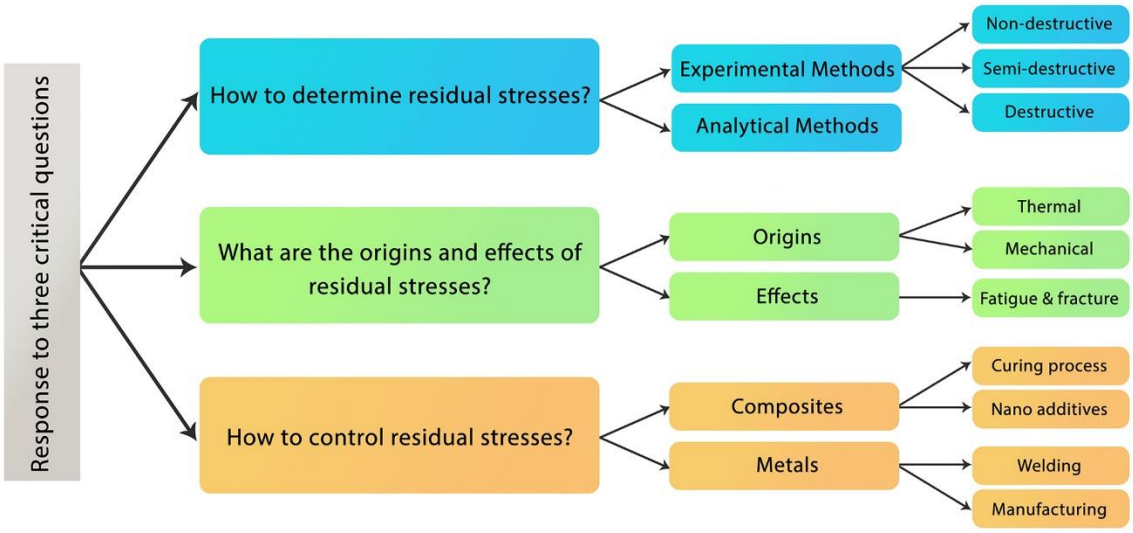

Fig. 1: Primary topics covered in this review.

2. Determination Methods

As mentioned earlier, residual stress assessment is of great interest among researchers in the engineering community. Several methods are used to determine residual stresses, including experimental measurement and analytical methods which will be discussed in subsections 2.1 and 2.2.

2.1. Experimental Techniques

Based on measurement depth and level of material removed, experimental techniques for assessing residual stresses can be divided into three main groups, namely ‘destructive’, ‘semi-destructive’, and ‘non-destructive’. Overall, non-destructive methods are relatively more expensive to perform and provide accurate results. Excluding the neutrons and synchrotron methods, non-destructive methods primarily measure residual stresses very close to the surface layer. Detailed information on the non-destructive methods can be found in [16].

On the other hand, destructive and semi-destructive techniques, also called mechanical techniques, are often cost-effective and need no high-tech equipment [17]. In these methods, residual stresses

are evaluated over several steps through the depth of specimens by removing the material incrementally. The associated deformations are simultaneously determined either traditionally via strain gauges or modernly by non-contacting optical methods such as Digital Image Correlation (DIC) or Moiré Interferometry [18]. Residual stresses can then be found using an integral-form equation that correlates measured strains to residual stresses. A detailed explanation of different optical methods for recording deformations in stress-relief techniques is presented in [19].

Over the recent years, new inspection solutions such as non-destructive evaluation (NDE) and structural health monitoring (SHM) methods have been developed. Not only are these methods cost-effective, reliable, and easy to implement, they also provide a high safety level during the testing procedure [20]. Mechanoresponsive materials that convert mechanical events into a measurable output that can be monitored non-invasively at a distance from the material are ideal candidates for stress-strain measurements. In particular mechanochromic systems that use a change in fluorescent output with mechanical deformation have been actively investigated for around fifteen years. While the field is still relatively small, many examples of such systems now exist [21]. These self-sensing materials can indicate their physical conditions such as stress, strain, temperature, and deformation and damage. A mechanochromic approach holds considerable promise for various applications, such as detecting residual stresses in molded plastics [22]. More information regarding this cutting-edge technology can be found in [21][23].

Due to less sensitivity to the type-II stresses that cause troubles in diffraction methods, stress-relief techniques have great potential to independently validate non-destructive measurements. Examples of this can be seen in various investigations in which contour and neutron diffraction methods are compared [24][25]. Mechanical relaxation measurements, nevertheless, cannot be repeated with the same samples and may need several specimens.

The chart below (Fig. 2) illustrates several widely used methods:

Fig. 2: Experimental techniques for assessing residual stresses.

Different experimental techniques were comprehensively presented in research by Rossini et al. [26]. Here we do not aim to introduce these in detail but to investigate different aspects of remarkable progress over the recent decade.

2.1.1. Contour Method

The contour method, first proposed by Prime in 2000 [27], was implemented to assess the longitudinal component of stress. Given that this method provides the visualization of residual stresses on the whole section of the assembly, outcomes of the contour method are commonly compared with those of the non-destructive neutron diffraction measurements [28]–[31]. The conventional contour method can assess only one component of residual stresses throughout the cross-section of a part. A new strategy in contour measurement of residual stresses was introduced by Pagliaro et al. in 2010 [32], in which the contour technique was developed for measuring multiple residual stress components by making multiple cuts (Fig. 3). This new technique was easier to implement than the multiaxial contour method and did not require an extruded cross-section. However, it had the disadvantage of evaluating different stress components on different cross-sections of the part.

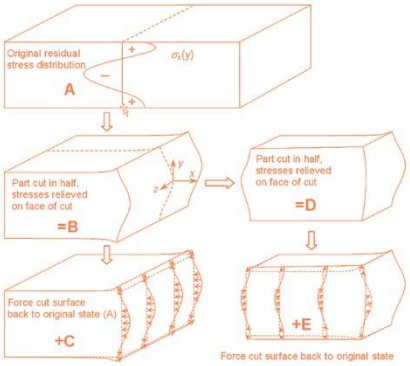

Fig. 3: The use of superposition principle for Contour method:

(A-C): traditional contour method, (D-E): multiple cuts. The two cut planes define x=0 and z=0. Adapted with permission from reference [32]. Copyright 2010, Springer

[32].

Brown et al. [24] compared the results of residual stress measurement in an electron-beam welded uranium cylinder via the contour and neutron diffraction methods. The results indicated that neutron diffraction assesses stresses approximately 50 MPa lower than the contour method. Possible sources of this error were discussed in this paper in detail. The contour method is insensitive to microstructural variation, such as those in the welding process. It is therefore seen that many studies associated with welding operations have employed the contour method for measuring residual stresses. The results of [33] demonstrated that the contour method could practically be applied for quantifying residual stresses in 8mm and 4mm thick friction stir weld (FSW) joints.

Cutting is the earliest and most critical stage in the contour method in which several sources of error could result in significant uncertainties in the measurement results. Research by Hosseinzadeh et al. in 2014 explored the controlling of the cut in the contour method [34]. Later, in 2017, two detailed studies suggested new perspectives for contour measurement of stresses. Two novel cutting configurations, a 4-cut double-embedded configuration with no clamping and a 5-cut double-embedded configuration with no clamping, were compared to a conventional 1-cut configuration with rigid clamping [35][36]. These cutting strategies could significantly mitigate the detrimental effects of cutting-induced plasticity, and their efficacy was verified through finite element (FE) and fracture mechanics analyses. Smith et al. [25] compared neutron diffraction and

contour measurement results in the linear friction welding process of specific alloys used in turbine and compressors. This quantitative analysis provided novel insights into neutron diffraction evaluation of residual stresses, highlighting that judicious selection of the beam width, height, and stress-free lattice spacing has great potential in reducing measurement errors and increasing accuracy. Contrary to ref. [24], the neutron data demonstrated slightly higher peak tensile stresses in the areas close to the weld interface than the contour method. Even though neutron diffraction and contour methods are extensively used for estimating residual stresses in the welding process, these methods are not capable of determining the evolution of welding-induced residual stresses. To address this challenge, scientists combined the mentioned methods with a FE method to investigate the full-field distribution of the residual stresses and back chipping effects in the thick plates [37]. It was clarified that residual stress distribution would be in an "M" shape across the width of the specimen. Regarding the back-chipping effect, it was found that it changes both the distribution shape and position of the peak residual stress value. Overall, residual stresses increase in line with the increase of back chipping thickness. As mentioned earlier, the contour method is based on specific stress-relaxation assumptions violated by cutting-induced plasticity. The effects of this on the back-calculated stresses were examined numerically in research by Sun et al. [38]. They came to these critical conclusions: (1) Significant errors in stress evaluation are produced in the areas in which plastic deformation is concentrated, and the edges of the specimens are most vulnerable to stress errors, (2) Errors in stress decrease and become insensitive to the cutting direction on the condition that adequate clamping is imposed. Olson and teammates provided a single measurement uncertainty estimator for the contour method, focusing on the two error sources, including the errors arising from noise in the measured displacement field and the ones associated with the smoothing of the displacement surfaces [39]. Very recent progress in the contour method has been made in two pieces of research in 2020 [40][41], where a new insight associated with the contour method was presented using a 3D scanner for determining cross-sectional residual stresses in structures with complex configurations. This advanced method allows a considerably reduced measurement time compared to the conventional method.

2.1.2. Slitting Method

The slitting method, also called crack compliance method, is another destructive method and has seen substantial developments since its first introduction in 1986. In this method, a slot is cut

incrementally through the depth of specimens (x-direction in Fig. 4), so that associated deformations can be measured and correlated to residual stresses. A slot with depth and width of ‘a' and ‘w’, respectively, and the specimen with ‘t’, ‘L’ and ‘B’ dimensions are shown by Fig. 4. Also, ‘l’ shows the strain gauge length.

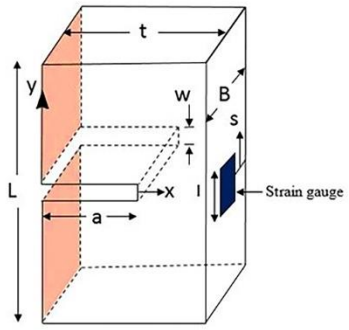

Fig. 4: Schematic of Slitting method. Adapted with permission from reference [42]. Copyright 2019, Elsevier.

The slitting technique has potential applications where components are manufactured by layer deposition methods, such as filament winding, laser cladding, and rapid prototyping [43]. Recently, a developed slitting method, called the slotting method, has successfully been applied to determine residual stresses in bone structures, particularly through-depth stresses in layers near the surface of bovine femurs [44].

The conventional slitting method determines the residual stress component normal to the slit face, while the strains associated with residual shear stresses are typically ignored in strain gauge measurements. This issue was taken into account by Shokrieh and Akbari [45][46]. Investigation of the influence of residual shear stress in carbon and glass fiber reinforced polymer composites (CFRP and GFRP), as well as steel specimens, revealed that the measured strains on the back surface are negligibly influenced by shear stresses, while on the top surface, strains associated with residual shear stresses are relatively significant and must be taken into account in calculations. Another drawback in slitting measurement is plasticity effects while cutting the samples. This is noticeable in areas where the residual stress level is high in comparison with the yield stress. Accordingly, the errors in slitting results are more significant in such areas [47]. As explained in [48], the slitting method employs an inverse solution to correlate deformations and residual stresses,

magnifying the associated errors through different solution stages. Remarkable progress in rectifying slitting-related errors was made by Can Aydiner and Prime [49], where a one-parameter correction was presented, providing a practical 3D constraint to reduce the root-mean-square (RMS) stress error from using 2D compliances. As mentioned earlier, the slitting method includes an incrementally cutting process in which stresses in each step may be influenced by the previous one. This cannot be ignored, particularly in the presence of high residual stress levels. To tackle this, a new cutting strategy to simultaneously measure stresses in two orthogonal directions was proposed by Mahmoudi et al. [50]. Also, the authors presented a modification to the so-called cross-slitting method in 2017 [51].

A more recent study introduced the repeated slitting safe distance (RSSD), which suggests the appropriate distance between slitting experiments to exclude the effects of the previous cuts, ensuring the validity of the next slitting steps. This method reduces calculations and helps to decrease experimental costs, specifically in structures with low thickness. Olson and Hill represented a combination of contour and slitting methods to the biaxial mapping of residual stresses in a quenched aluminum bar. Both the longitudinal and transverse stresses were seen to have a paraboloid distribution, with tensile stress in the center of the cross-section and compressive stress through the edges, which is consistent with the typical residual stress profile in quenching [52]. Another disadvantage of the slitting method is that elastic deformations recorded by strain gauges are directly used in residual stress calculation, leading to severe errors and high scattering in final results [53]. Shokrieh and Kamangar [54][55] suggested an Eigen strain approach in which pure measured strains and conventional polynomials in residual stress calculations were replaced by a constant and invariant strain distribution field, and a superposition method, respectively. To overcome the difficulties of implementing the DIC technique, they proposed a robust procedure based on the Eigen strain approach for using the DIC technique combined with the slitting method while excluding the rigid body motion and rotation artifacts from the obtained displacements [56]. The results showed that different slitting increments appear to induce different rigid body motions and specimens' rotations. The proposed method was able to eliminate all these different shears and stretches in the images simultaneously.

2.1.3. Hole Drilling Method

Hole drilling is a widely-used method for measuring residual stresses through the depth of specimens and includes different types, such as “central or blind hole drilling” and “incremental or deep hole drilling” [57]–[59]. The ASTM Standard Test Method E837 associated with the hole drilling technique was introduced in 1981. This method is similar to the slitting method in many aspects. However, damage caused by this method is limited to the drilled area; therefore, it is classified as a semi-destructive technique. Even though this method may not assess stresses as deeply as the slitting method, its convenient practical implementation and available standardized testing procedure make it a method of choice over other ones [60][61]. A schematic of clockwise strain gauge rosettes in this method is shown in Fig. 5. The positive x-direction lies along the axis of gauge 1, and the negative y-direction lies along the axis of gauge 3, and a circular hole is drilled at the center of that.

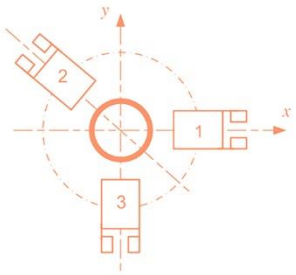

Fig. 5: Typical strain gauge configuration in hole drilling method. Adapted with permission from reference [1]. Copyright 2014, Elsevier.

An excellent review of advances in hole drilling method before 2010 can be found in [19]. To achieve the best compromise between low sensitivity to random error and the capability of reconstructing the correct function of residual stresses, Petrucci and Scafidi [62] proposed a new calculation method based on the Newton-Raphson technique for the solution of the inverse problem in the hole drilling method. The incremental hole drilling technique could effectively assess residual stresses in fiber metal laminates (FMLs) [63]. Also, the reliability and challenges of the hole drilling method in determining residual stress in polymeric materials have been pointed out in two pieces of research by Magnier and teammates [64][65].

Similar to other stress-relief measurement techniques, the DIC has vastly implemented along with the hole drilling method [66]. However, a challenge to do so is that DIC has barely sufficient sensitivity to identify the relatively small displacements caused by hole drilling. Also, the

measurements are often prone to artifacts that may be larger than the displacements of interest. Schajer et al. [67] reported a new computational strategy for hole drilling-DIC measurement of residual stresses, taking advantage of the large quantity of data available from full-field images to rectify the influence of modest deformation sensitivity of DIC measurement as well as minimizing human guidance. In 2014, a modified hole drilling-DIC procedure called integrated DIC (iDIC) technique was introduced [68] in which 'generic' displacement functions commonly used to determine displacement profile around the measurement area were replaced with problem-specific ones so that stress components became the unknowns of the problem and a single-pass analysis could be performed. Despite the significant advantages, such as high accuracy, robustness, and simple implementation, the method faces serious problems when applying the Integral Method to estimate depth-dependent residual stress components. Later in 2019 [69], two alternative approaches were suggested to address this drawback. The first one included employing the direct solution of the triangular linear system for incrementally identifying the stress distribution, and in the second one, a global Spatio-temporal minimization considering all the acquired images was proposed. In practical terms, residual stresses in such large and industrial structures as bridges, railways, buildings [70], and microelectronic packages [71] are measured via hole drilling method, given its semi-destructive nature and less damage caused compared to destructive slitting or contour methods. In [70], a method including hole drilling combined with DIC was explored where residual structural stresses were effectively characterized. The method was based on using a calibration measurement to clarify the equivalent residual stress profile that exists for a given structural element type. This, nevertheless, was not a systematic way of estimating the equivalent residual stress profile, and an obvious drawback was the need for calibration measurement, which could be efficiently enhanced using FEA models. Ref. [72] highlights the importance of calibration coefficients in hole drilling measurement, particularly the influence of Poisson's ratio, which could make a considerable difference of 17% in obtained calibration coefficients, consequently, final stress approximation. Another significant improvement in this circle was made in 2016, where a new systematic calibration approach using multiple case-specific calibration functions for residual stress measurement in highly anisotropic materials was reported and successfully verified [73]. Schajer and Abraham also extended the conventional calibration constants, taking into account the local bending effect in finite-thickness materials, resulting in the possibility of using the hole drilling method in specimens of a wide range of thickness [74]. A very recent study in 2020 provides

a novel two-variable polynomial formulation to represent hole drilling calibration data in which hole diameter and specimen thickness are taken into account. This study reduces the 231 coefficients for a 20-step hole drilling process to efficient 15 numerical coefficients, opening up a new horizon for systematic, time-efficient and specified calibration data calculation for future studies [75].

Another crucial area in the development of the hole drilling method is the drilling process itself [76] and other experimental setups associated with strain gauge rosettes. For example, applying the orbital drilling technique with standard six-blade bits would lead to the highest quality in hole geometry and centricity to the center of the strain gauge rosette [64]. A study on the influence of drilling parameters [77] suggested that the common conception that ultra-high rotation speeds are required to achieve accurate results may not always be the case. It was also demonstrated that the bit diameter and hole depth have a subtle effect on the accuracy of measurement results. Remarkable progress in strain gauge design in the hole drilling experiment was recently made [78], where circumferential strain gauge rosette could detect interior residual stresses to nearly double the depth possible when using a standard radial rosette. There is, nevertheless, the disadvantage of reducing strain sensitivity, especially deviatoric (shear) stresses. Smit and Reid [79] proposed a new method to approximate residual stress distribution in laminated composite materials using power series expansion of separate Eigen strain functions in each ply orientation. The method showed great potential for materials in which considerable variation of residual stresses exists within a single ply but lacked when several layers with the same angles are stacked together. Later, they extended the power series expansion to obtain the best estimation of the residual stress distribution in the hole drilling technique [80]. In 2020, they also applied the Tikhonov regularization with incremental hole drilling on a GFRP laminate for the first time, concluding that the application of the Tikhonov regularization method results in the reduction of stress uncertainties [81].

2.1.4. Ring Core Method

The ring core method is a semi-destructive technique being introduced in 1951 and officially patented in 1988. This was a response to practical restrictions associated with the hole drilling method. It consists of milling a minor circular groove around the point of interest; then the residual stress is determined from the surface deformations of the core; in this case, while in the hole-drilling method a part of the material is removed from the center and outside strains are monitored,

in the ring-core, the material is removed from the outside, and the inside is monitored in search of relaxed strains. Nevertheless, in the ring core method, the specimen will not destroy entirely and may be used for further applications. Indeed, this is one of the few mechanical approaches that can be restarted (by removing the core and re-installing the strain gauge rosette). Thus, it can measure residual stress at a significantly greater depth than other methods and is reported to be more sensitive during strain measurement [82].

On the other hand, it appears to suffer from impractical problems such as the need to disconnect the strain gauge wires to allow the ring drilling to proceed. This can be addressed by replacing the strain gauge rosette with an optical (interferometric) technique [82]. Another drawback in calculations is the necessity of derivative evaluations with relatively high accuracy [83]. Overall, the number of publications related to this method is relatively less than other mechanical techniques, i.e., slitting, hole drilling, and contour methods. Zhu and teammates combined the ring core and DIC methods to characterize residual interfacial stresses in thermal barrier coatings at the microscopic scale. The cutting procedure was implemented by the focused ion beam (FIB) milling [84]. It must be pointed out that the micro-scale FIB-DIC ring core technique dated back to 2009 [85]. It was remarkable progress in developing the conventional ring core method, where a number of its limitations and drawbacks were successfully addressed. The FIB-DIC ring core method has a vast application in dental sciences, as discussed in section 3 [86]. It is also applicable for characterizing residual stresses in polycrystalline bulk materials at the micro-scale [87]. Some interesting research in this field has been published by Salvati and Korsunsky [88]. They accomplished the FIB-DIC ring core milling approach to characterize inter-and intra-granular residual stresses induced by plastic deformation in aluminum alloys. Error propagation associated with measurement uncertainty was also considered in this analysis, and results of experiments and numerical modeling showed a 29% disagreement for randomly distributed crystal structure, while this was seen to be 24% for a realistic crystal texture of the material [89]. Recent studies by authors on the residual stress depth profiling at the nanoscale in FIB-DIC ring core method presented the reconstruction of the full in-plane residual stress tensor as a function of milling depth, which eliminated the main limitations of classic integral methods. More information and complete review of various methodologies based on the FIB-DIC ring core approach can be found in [90]–[93].

Menda et al. investigated the effects associated with the geometric shape of the cutter in the ring core measurement. It was indicated that the maximum error exists at the first milling steps, and the ring core method can be used from the depth of 1 mm. Another method for shallower depths should be implemented subsequently [94]. Research in 2016 presented the list of the primary error sources and the effects of each source on the calculated residual stresses in the ring core method. Also, a systematic procedure for the residual stress uncertainty estimation was implemented in this paper [95]. Moharrami and Sadri's outcomes suggested that as opposed to the hole drilling method, in surface residual stress determination by the ring core technique, the plasticity-induced errors would have higher values and can be reduced by increasing the ring depth. It was also clarified that these errors are a function of the ring geometry, material properties, and maximum residual stress magnitude [96]. Bouffioux and teammates measured residual stresses on long rolled profiles conducting X-Ray diffraction (XRD), ring core (with strain gauges), and sectioning methods. They reported that the ring core measurement results agree with numerical models, both in longitudinal and transverse directions, suggesting that this method is well adapted to this kind of piece [97]. Also, the ring core method has successfully been used for determining residual stresses induced in the welding process [98]. Researchers have extended the coefficients of a well-known integral method to determine non-uniform residual stresses in the ring core technique. Subsequently, the eccentricity effect was taken into account, which turned out to be negligible due to the symmetry of the problem [99].

2.1.5. Curvature Measurement Method

Another non-destructive strategy for estimating residual stresses, which is relatively more straightforward and less expensive than other non-destructive methods, is to measure the curvature or cured shape of structures based on some preliminary works in 1981 by Hyer [100]. This method provides a general understanding of residual stress value and is based on a principle according to which residual stresses directly affect the curvature, meaning that the larger curvature is, the more residual stresses are locked in laminates. From a structural point of view, composite structures could be divided into two groups, namely ‘symmetric’ and ’asymmetric’. It is a well-established fact that asymmetric laminates will develop a particular cured shape when exposed to thermal loading conditions, while symmetric ones will always be flat [100]–[102]. Accordingly, this method can only be used for residual stress analysis in asymmetric structures. Moreover, the method

cannot determine residual stresses at a particular point or depth of composite structures but can give an essential insight regarding the residual stress quality; in fact, this is primarily useful for observing the changes in residual stresses rather than determining the exact value of them. Shokrieh et al. [103] suggested that residual stresses in composite materials can be controlled with the addition of carbon nanofibers (CNFs) (Fig. 6(a)). As shown by Fig. 6(a), the curvature in the sample with 0% CNFs (with higher residual stress value) is larger than the ones with 0.5% and 1% CNFs. Ghasemi and Mohammadi [104][105] studied the influence of various parameters, including thickness, curing temperature, and CNF percentage on the cured shape of cross-ply fiber-reinforced composite laminates. Based on experimental findings, a developed micromechanical model to study the curvature and residual stresses was proposed. In recently published studies by Tabatabaeian and Ghasemi [106]–[108], curvature response of CNF/glass fibers/epoxy composites was investigated considering the influence of resin type, thermal fatigue, stacking sequence, and CNF reinforcement. Also, residual stress relaxation and curvature changes over time were examined and reported. The results of these works revealed that depending on the resin type and curing condition, the addition of CNF can cause different reactions to the cured shape of various composite laminates. Moreover, it was established that curvature changes and residual stress relaxation over time are highly dependent on the CNF content and number of exposed thermal cycles. This area appears to need further experimental and analytical investigations in future studies so that a better prediction of residual stress quality based on curvature response could be achieved.

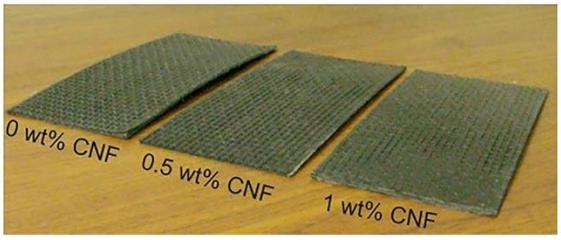

(a)

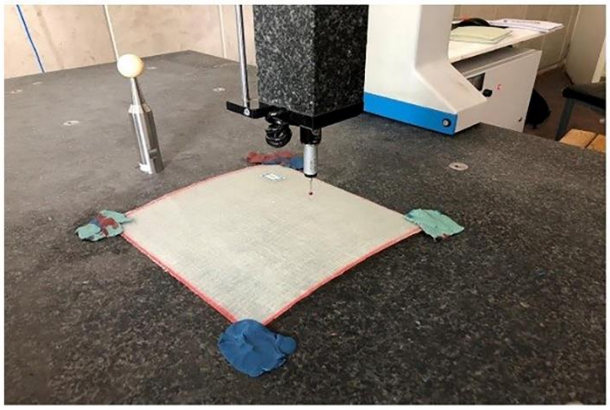

(b)

Fig. 6: a) Effect of CNF percentage on the curvature of asymmetric $[0_2/90_2]$ laminated composites. Adapted with permission from reference [103]. Copyright 2013, Elsevier., b) Measuring curvature via Coordinate Measuring Machine (CMM). Adapted with permission from reference [106]. Copyright 2019, Elsevier.

2.1.6. X-Ray Diffraction Method

XRD is a practical and non-destructive method used to determine the in-situ strains in a material in which the crystalline planes are considered as strain gauges . In this method, the strains and stresses are correlated based on the classical theory of elasticity, and the equation of Bragg's law is the basic idea of all residual stress measurements using X-Ray diffraction methods [109]–[111]. The cones come into view as circular intensity rings in the transmitted diffracted beams, known as Debye rings. A two-dimensional detector that is normal to the incident beam records the rings (Fig. 7). The application of stress changes the interplanar distance, leading to the distortion of these Debye rings at the detector. The degree of distortion in the direction of applied stress provides a reasonable estimation of the lattice strain. The schematic of strain measurement in the XRD method is demonstrated in Fig. 7.

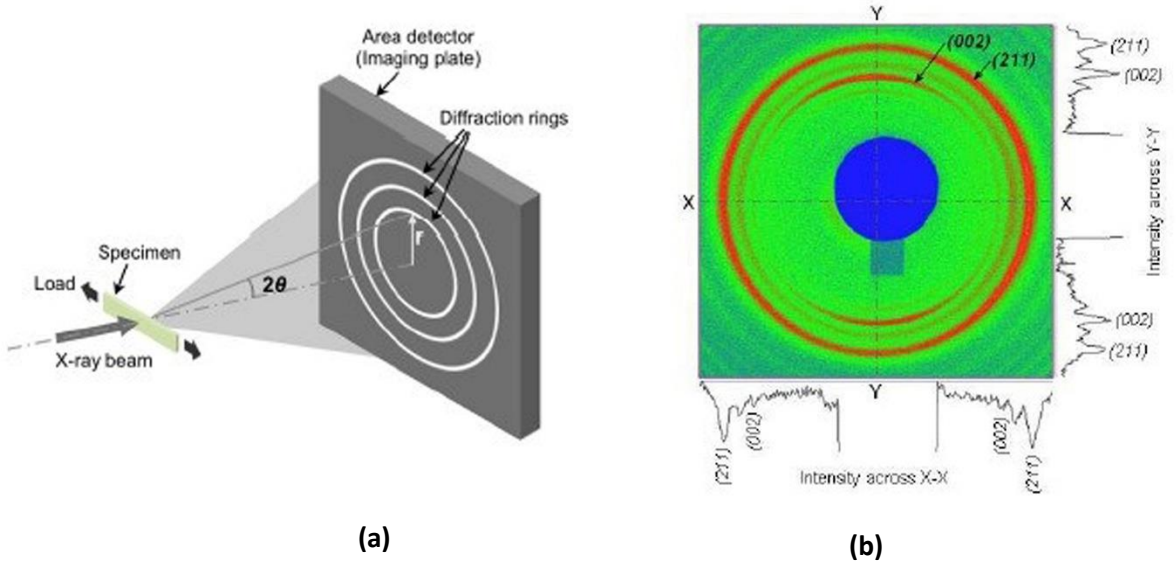

Fig. 7: a) Schematic of the XRD experiment, b) Two-dimensional diffraction pattern recorded in the detector. The intensity rings present diffractions from different lattice planes of the crystal. Adapted with permission from reference [112]. Copyright 2011, Taylor & Francis.

Robinson and Redington used the XRD method to measure near-surface residual stresses and related them to the strength and hardness properties in heated treated aluminum alloys [113]. Over recent years, X-ray diffraction techniques have also gained increased attention as useful non-destructive tools for investigating the nanostructure of bones and biological systems [112]. Righetti and teammates made recent progress in the XRD technique in 2020, where they developed a multireflection grazing incidence X-ray diffraction (MGIXD) method. It was established that MGXID is a helpful tool to assess the residual surface stresses in milled and shot-peened aluminum alloys, with the potential to guide the optimization of parameters in both milling and shot-peening processes. Moreover, it provides properties commonly undetected in conventional residual stress methods [114]. Hizli and Gur [115] introduced a new technique, called Magnetic Barkhausen Noise (MBN), to nondestructively measure residual surface stress in carburized steels. Comparison of the MBN measurement results with those of the XRD method revealed that while both techniques give a similar tendency for residual stress variations, the MBN method is much faster than the XRD, and from the industrial point of view, the MBN method could be a strong candidate for non-destructive monitoring of residual stress variations qualitatively in the carburized and tempered steels. It should, however, be noted that in the case of synchrotron experiments, in-situ measurements with an exposer time of 0.1 second are also possible, with a higher local accuracy than MBN methods.

Various research on the residual stress characterization using synchrotron x-ray-based methods was accomplished by Salvati and teammates [116]–[121]. The residual stress measurement principle in synchrotron XRD (SXRD) is similar to the standard XRD, while SXRD uses the polycrystalline lattice of the material as an atomic strain gauge and relies on accurate measurement of the change in separation of atomic lattice planes in polycrystalline materials due to stress [122]. The penetration depth in SXRD is much higher than laboratory-based X-rays, thus providing high spatial resolution 3D maps of the strain distribution to millimeter depths in engineered components. The disadvantage of this method is that it is only applicable to polycrystalline materials [123][124].

Short-wavelength X-ray diffraction (SWXRD) is a type of XRD that does not require neutron or high-energy synchrotron radiation sources, showing excellent potential for investigating the distribution of internal residual stresses in welding procedures [125]. A well-organized summary of diffraction residual stress analysis is presented by Manns and Scholtes [126].

More applications of non-destructive neutron diffraction and XRD measurement strategies are discussed in the next section.

2.1.7. Ultrasonic Method

The Ultrasound method is a non-destructive, through-thickness stress measurement technique. The presence, direction and magnitude of the residual stresses cause a change in the speed of ultrasound waves travelling through material. In this case, residual stresses can be quantified by carefully determining the change in time of flight of an ultrasound wave traveling through the stressed and unstressed regions of that material. It must be noticed that the ultrasound waves are sensitive not only to stress variations but to microstructural and temperature variations [127][128]. The change in time of flight, Δt, of can be written in terms of the four effective parameters:

$$\Delta t = \Delta t_{AS} + \Delta t_{RS} + \Delta t_{T} + \Delta t_{M} \quad (1)$$

Where Δt_{AS} is the change in time-of-flight associated with applied stress changes, Δt_{RS} is the change in time-of-flight due to residual stress changes, Δt_{T} is the change in time-of-flight because of temperature changes and Δt_{M} is the change in time-of-flight due to microstructure changes. It is often challenging to take into account the microstructural variations in the above equation. Ultrasonic measurement has some advantages, such as being non-destructive and applicable to a wide range of materials. Nevertheless, it suffers from the following disadvantages: it is sensitive to microstructural changes; it is only applicable to components with a high-quality surface finish and cannot be applied in complex-shaped structures; it is challenging to specify the spatial resolution by this method [129][130]. Research in the literature shows that ultrasonic method is a popular technique, especially to determine welding-induced residual stresses [128][129].

2.2. Analytical Methods

As stated earlier, experimental techniques are identified as primary methods to characterize residual stresses. Nevertheless, developing analytical and FE models could help to predict residual stress quality at relatively lower costs and in a time-effective way [131]. A major drawback in these methods is that all the actual conditions cannot be modeled or simulated, which causes errors in predictions. Shokrieh et al. compared the slitting method and classical lamination theory (CLT) to determine macro-residual stresses in composite materials [132]. As shown by Fig. 8, the CLT

overestimates the magnitude of residual stresses. This can be attributed to the fact that there is no consideration regarding the temperature-dependency of thermo-mechanical properties of the laminated composites in this theory, particularly over the curing process [132].

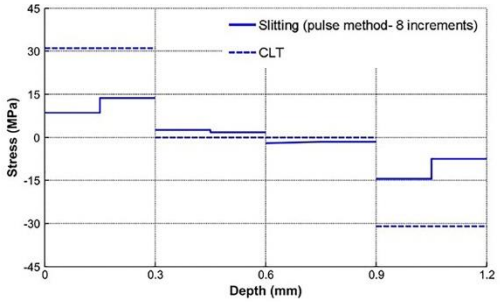

Fig. 8: Comparison of experimental and theoretical results in determining residual stresses for $[0_4/90_4]_s$ polymer composite laminates. Adapted with permission from reference [132]. Copyright 2012, Elsevier.

In another study, the ring core measurement results were compared to those of CLT. It was observed that there is an error of 16% and 8% between the ring core and CLT results for symmetric cross-ply and symmetric quasi-isotropic laminates, respectively [133]. As seen in these examples, there are some differences between the outcomes of experimental measurements and analytical studies. Zhang et al. developed a prediction model of the curing residual stress in CFRP/Al adhesive joints based on CLT. The model was successfully verified through comparisons with experimental and FE results [134]. Their model was based on the following assumptions: 1) residual stress is plane stress, 2) residual stress torque does not exist, 3) adhesive is an elastic material, and 4) CFRP and Al layer have the same deformation [134]. In two pieces of research, Shokrieh and teammates developed the simulated central hole drilling (SCHD) and slitting methods [55,57], which are fundamental sources for simulation of mentioned procedures. Based on the CLT, an analytical framework to predict residual stresses in terms of temperature changes and thermal cycling conditions was developed in [135].

The accuracy of predicting the curing residual stress relies on a proper constitutive model containing various influential factors, namely “thermal expansion”, “cure chemical shrinkage”, “layers architecture” and “material degradation or relaxing during curing”. In addition to the CLT, residual stresses in polymer composites can be analytically determined via different micro-

mechanical methods, namely “elasticity solution” [136], “cylinder theory” [137], “Elshelby theory” [138], “energy method” [139], “the cure hardening instantaneous linear elastic (CHILE) model” [140] and “visco-elastic model” [141]. Given the two-dimensional nature of the elasticity theory, the out-of-plane stress components and the material anisotropy and fiber length are not considered in this method. The cylinder theory fits the plane-strain conditions, meaning that this solution cannot be used for fibers of finite length. Moreover, the Eshelby theory estimates the stress and minimum strain energy of inclusion (or inhomogeneity) transforming in a constraining matrix. The elastic models coupled with the CLT are capable of predicting residual stresses in thin laminates. Nevertheless, they lack in thick laminates, where the elastic models may not capture the complexity of temperature and degree of cure. The energy method is more favorable among the engineering community since it can consider more general conditions, i.e., physical, thermal, and mechanical parameters on the thermal stress fields. Also, as opposed to other methods, residual stresses can be obtained directly via this method [142]. The CHILE model has shown a good potential to predict the final stress as well as deformation of composite laminates. It has the advantage of simplicity in modeling and FE implementation while considering the effects associated with temperature and degree of cure gradients over the curing process. On the other hand, this model suffers when it comes to the effect of stress relaxation at elevated temperatures [143]. In visco-elastic models, the visco-elastic characteristics of polymer matrix such as strain creep and stress relaxation, specifically at high temperatures, are considered. Aiming at the study of the residual stress development in autoclaved composite laminates, a research in 2015 proposed a three-dimensional differential thermo-visco-elastic constitute law and FE-based subroutine taking into account the CTE changes, chemical shrinkage, and stress relaxation during the curing process. This differential constitutes law was proved to be more suitable than previous integral constitute laws [141]. Authors of [118] employed energy and FE methods to study the influence of poor adhesion between matrix and fiber on the micro residual stresses to determine the effect of some influential parameters on the residual thermal stresses in polymeric composites. In particular, the effects of Poisson’s ratio, CTE, and modulus of elasticity were taken into account. It was observed that compared to the energy method, the FE solution yields a higher magnitude of residual stresses. Also, it could not satisfy the stress-free condition at the fiber end. Merodio et al. proposed a theoretical analysis to scrutinize the influence of residual stresses on the elastic behavior of materials exposed to finite elastic deformations. A three-dimensional problem of extension and

torsion of a circular cylinder with a prototype strain-energy function and residual stress distribution was examined in this paper [144].

The Wang-Rose and Van Bameveld-Fredell models are two coherent models for theoretically predicting the curing residual stress in the heterogeneous composite structure. The former was developed based on the Rose model and did consider the heating and cooling processes associated with the curing system in the calculation of residual stresses. The latter can be used for a broader range of structural forms, where an effective thermal expansion coefficient is introduced to predict residual stresses accurately. In this model, however, there is a shortcoming that no assumption is made regarding the difference between cooling and heating in the curing process [134]. The results of experimental research by Liu et al. revealed that the residual stress in the silicon film for a silicon-on-sapphire system is dependent on the film thickness [145]. This could not, nevertheless, be explained by merely the CTE mismatch. Later, in another paper [146], they developed a FE model to thoroughly investigate the contribution of the CTE and lattice mismatches and misfit dislocations in the various mechanisms of the residual stresses in thin film-substrate systems. The proposed FE model could satisfactorily predict the residual stresses, coupling the effects of the three mentioned factors. Sedighi et al. established an analytical solution for predicting residual stress caused by roll bending in bi-layer Al-Cu sheets. In this formulation, the neutral axis movement due to different elastic moduli of two layers was taken into account, and the results were in good agreement with those of slitting measurement [147]. In work by Song and teammates, process-induced residual stresses in double-ceramic-layer thermal barrier coating systems were theoretically predicted using a new model. The influence of critical process parameters on the residual stresses was also investigated, and the model was successfully verified through comparisons with FE results [148]. In a recent study, Jafarpour et al. investigated the residual stress distribution in CNF/epoxy nanocomposites with different CNF patterns, employing Halpin-Tsai-Schapery (HTS) and Mori-Tanaka-Schapery (MTS) and FE models. The results suggested that HTS and MTS models can adequately predict residual stresses in nanocomposites with random CNT distribution patterns, while for specific patterns, the FE model is recommended [149].

3. Origins and Effects

A literature review indicates that the concept of “residual stress” is widely discussed in various fields of science, including mechanical, civil, metallurgical, chemical, electronics, medical, and

dental sciences, etc. After a careful investigation through available publications, the authors found six main areas dealing with residual stresses, which can be classified into two primary groups, namely “origins” and “effects”. These main areas and associated keywords are illustrated in Fig. 9.

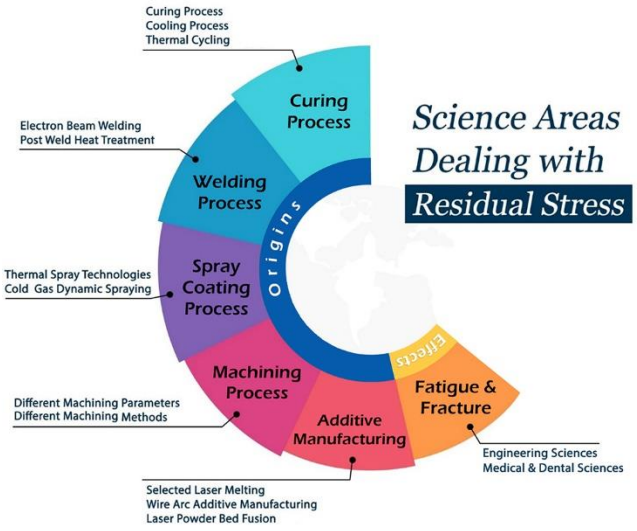

Fig. 9: Main science areas related to the residual stress.

In the following, five areas are covered in detail. Given the high volume of publications related to the measurement and mitigation of residual stresses in different additive manufacturing processes, this area will require a specific investigation and not be discussed in this paper.

3.1. Origins

3.1.1. Thermal

a) Curing Process

As mentioned earlier, a primary cause for the creation of residual stresses is an abrupt or cyclic change in the temperature field, meaning that the residual stress distribution is strongly dominated by plasticity due to thermal misfits which may happen in curing [150][151], cooling [152][153], thermal cycling [154][155] and heat treatment [156] processes. On the other hand, a well-established procedure for removing residual stresses induced on the surface of structures after the surface modification processes, without microstructural change, is to perform low-temperature heat treatment [157]. For example, research by Jiang et al. [156] illustrates that the residual stress in AlSi10Mg alloy drops

gradually and stabilizes with the decrease in heating temperature, reaching a minimum at 250℃. In building materials, as established in [158], the residual compressive strength of heated concrete decreases significantly for temperature exposure over 400℃, and a considerable reduction rate of 89.26% could be achieved at 800℃.

The influence of cooling rate on the residual stresses in Fe-2.1B (wt%) alloy was characterized in [159], showing that the compressive residual stresses associated with cooling rates of 0.5 and 30 K/s are 18% and 36% higher, respectively, than those induce under the cooling rate of 0.1 K/s. This highlights the crucial role of the cooling process in achieving optimal microstructural properties such as residual stresses in alloys. Robinson et al. applied the cold compression method to reduce residual stresses in the aluminum alloys, concluding that cold compressions of 1.4% tend to alleviate the bulk of the residual stresses. However, greater cold compressions are likely to be beneficial in decreasing the range of the remaining residual stresses [160]. Moreover, it was revealed that surface compressive residual stress is influenced by the implementation of cold compression to a higher degree than the interior tensile stresses [161]. Accomplishing slitting technique coupled with statistical analyses, Asghari et al. [162] scrutinized the impact of the cooling condition on the residual stresses of CFRP shells, reporting that temperature differences between curing and cooling conditions induce thermal shock, resulting in building up of high residual stress levels, which, in turn, accelerates the structural failure. Simultaneous cooling conditions and CNT-reinforcement effects were studied in [163], indicating that the influence of cooling conditions on the residual thermal stresses becomes more significant when the CNT percentage decreases. A recently published study regarding the cooling effect on the ply-scale residual stresses and curvature in asymmetric GFRP composites [164] has presented a model based on the modified laminate theory, for the first time, accounting for the development of material thermo-mechanical properties during cooling. It is worthwhile noticing that there might be constraints in the cooling process of materials; for example, some alloys could become significantly harder when cooled to particular temperatures. According to [165], aluminum alloy 7449 is 60% harder at -196 ℃ compared to the as-quenched condition. Despite the mentioned progress, further investigations in this realm, most specifically in providing efficient theoretical models to consider the cooling effect and reach optimal state, seem to be needed.

Several parametric studies regarding the influence of thermal cycling on the residual stresses of polymeric composite materials were conducted by Tabatabaeian et al. [42][106][107][135][166]. In [135], a new algorithm based on classical laminate theory to study the influence of temperature change and thermal cycling on the residual stresses and failure of various stacking sequences was developed. It was established that, overall, there is a meaningful relationship between the number of thermal cycles and residual stresses; also, residual stresses decrease with increase of temperature (Fig. 10).

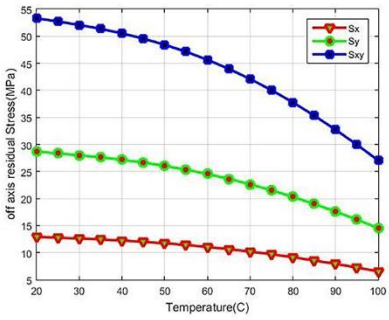

Fig. 10: Residual stresses in terms of temperature variations in $[0_2 / \pm 45]_S$ laminates. Adapted with permission from reference [135]. Copyright 2018, Sage.

The slitting technique, along with the Tikhonov regularization method and FE analysis [42][166], suggested that regardless of laminate architecture, residual stresses drop when composite materials go through thermally cycled fatigue conditions (Fig. 11). This can be attributed to the completion of the curing process over cyclic temperature fluctuations. Moreover, it was reported that, under temperature changes, residual stress variations along the specimen thickness decrease as a result of CNT addition [107]. Fig. 11 also demonstrates that the symmetric nature of lay-up arrangement in composite materials exposed to thermal cycling could help to mitigate the magnitude of residual thermal stresses.

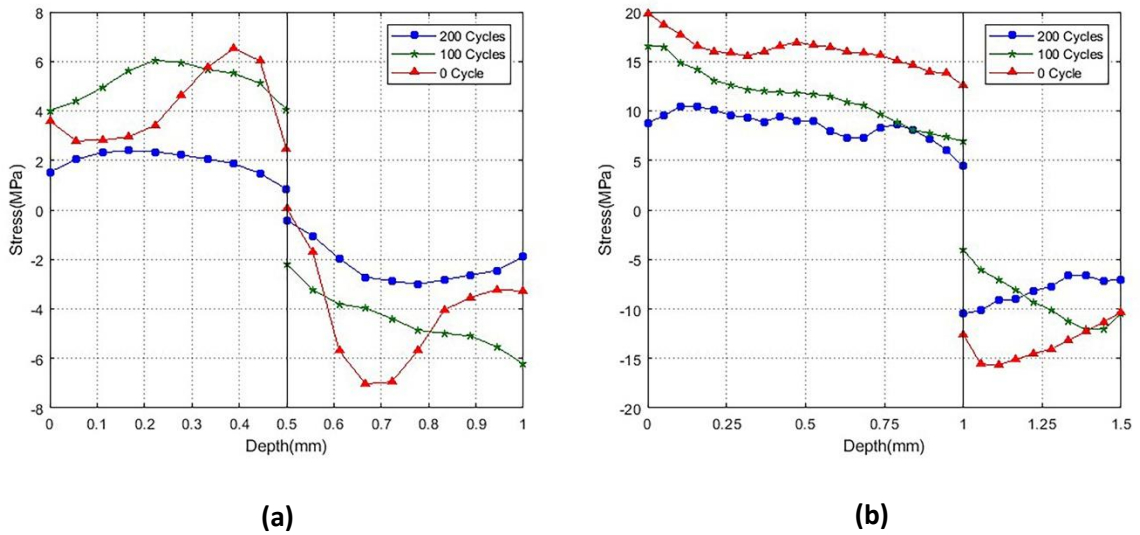

Fig. 11: Decrease of through-thickness residual stresses in composite materials exposed to thermal cycling: a) Symmetrical configuration $[0_2/90_2]_S$, b) Asymmetrical configuration $[0_4/90_4]_T$. Adapted with permission from reference [166]. Copyright 2019, Elsevier.

b) Welding

Welding is a well-established technique in industrial assembly to join elements made from similar or dissimilar materials. A prime example of this can be seen in nuclear, thermal fertilizer, and chemical power industries in which different structural components, piping, and pressure vessels are joined together via the welding process. As confirmed by many publications [167][168], a severe problem that engineers in welding technology are dealt with is to measure welding-induced residual stresses. In practice, localized heating and quick cooling in the joint region during the welding operations tend to cause a sophisticated distribution of undesirable residual stresses with magnitude approaching yield strength, which, in turn, may lead to unwanted distortion in the whole welded structure as well as reducing fatigue life by increasing fatigue, corrosion, and creep stress crack growth rates [169]. Post-weld heat treatment (PWHT) could sometimes mitigate the residual stress state [170]. In this process, welding residual stresses are relieved by converting elastic strains into creep strains. The role of creep on the residual stress relaxation during the PWHT is explained in [171]. A study on the comparison of residual stresses in a P91 steel pipe weld before and after PWHT suggested that the highest tensile residual stresses at heat affected zone (HAZ) decrease from 600 MPa (before PWHT) to 120 MPa (after PWHT) [172]. This method, nevertheless, may

have detrimental metallurgical effects (sigma phase precipitation) for welding-related applications. For example, rational choice of the ambient temperature and holding time of the PWHT process may maximize the creep strains, which, in turn, lead to the most significant residual stress relief; however, the cooling plan of the PWHT process and microstructural changes accompanying the relaxation process must be precisely considered. Otherwise, the PWHT may bring detrimental effects [173]. This is thoroughly analyzed in [174], where a methodology for optimizing the heat treatment in welded components is provided. The nature of welding-induced residual stresses in the weld fusion zone and HAZ of P91 pipes has mostly been found to be tensile [175]. Ramjaun et al. reported that weld filler alloys might help reduce residual stresses in multi-pass welds to some extent [176].

Overall, the main factors associated with the formation of welding-induced residual stresses can be classified into three types, namely '*material properties*', such as thermal conductivity and work hardening coefficient, '*design-related parameters*', such as the shape of joint and plate thickness, and '*fabrication-related variables*', such as welding method, preheating temperature and deposition sequence. Outcomes of [177] suggested that the welding sequence does not significantly affect the distribution of longitudinal residual stresses but has a considerable influence on the peak value of the residual stresses. This was also reported in [178], where authors studied the welding deposition and heat input effects on the residual stresses. Fu et al. [179] represented a 3-D FE model to characterize the welding sequence effects on the residual stresses, making some advice on the optimized welding sequence in T-joint welds.

Even though the magnitude and distribution of residual stresses could be highly affected by the entire welding process [180], when the influence of individual parameters is specifically scrutinized, there seem to be some contradicting reports causing uncertainty in their application in real-life cases. For example, as [181] suggested, it is commonly expected that the value of heat input has an inverse relation with the magnitude of residual stresses, meaning that the lower heat input is, the higher stresses are formed at the weld joint. Surprisingly, however, this is not always the case because the heat input is a mixture of welding travel speed and applied current and voltage; thus, its effect becomes less straightforward [182]. Accordingly, the general trend mentioned above might vary depending on the particular conditions. A thorough analysis for any given real-life case appears to be essential. As shown by Fig. 12, weldability of P91 steel welded pipes is another in-

service example of the above conclusion in which hydrogen-induced cracking (HIC) is a serious concern, where a combined impact of high residual stress, sensitive microstructure, and sufficient hydrogen level would result in catastrophic failure in welding region [175].

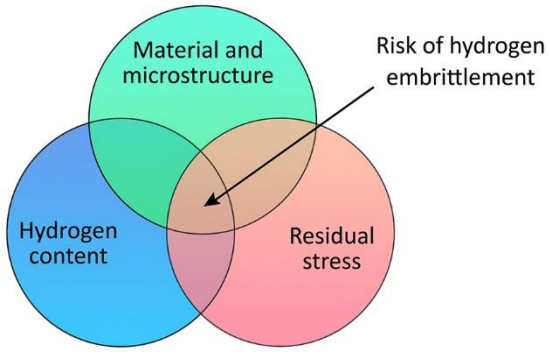

Fig. 12: A schematic of primary conditions that affect the weldability of steel pipes. $[0_4/90_4]_T$. Adapted with permission from reference [175]. Copyright 2018, Springer.

Hill et al. [183]–[185] explored the precision of contour, hole drilling, and neutron diffraction methods for biaxial residual stress mapping in dissimilar metal and stainless-steel welds, observing significant amounts of tensile residual stresses near the interface between the weld and based metal in the dissimilar metal weld. Findings of research regarding the influence of back chipping on the residual welding stresses signified that back chipping could change the distribution shape of residual stresses and affect the position of the peak value. Moreover, the increase of the back chipping thickness leads to increased residual stresses during the welding process [37].

Commonly, the elements subjected to the welding operations might have had previously experienced other manufacturing processes, such as machining, which could potentially cause an existing residual stress field. This is also the case for weld repairs, where the procedure is conducted to fix an anomaly created during the manufacturing stage or to repair in-service-related damages [186]. Residual stresses induced by repair welding could decrease the average fracture toughness of welded specimens by 40% [187]. Salerno et al. investigated the interaction between the pre-existing residual stresses with those created during the welding procedure, suggesting that if the study has to do with evaluating the local stress distributions, given the negligible effects of pre-existing stresses, they can be neglected in welding simulation analyses. On the other hand, if

the research concerns determining the distribution of welding residual stresses globally, any pre-existing stresses in the component should be taken into account in FE simulations [188].

In addition to two main methods for estimating residual welding stresses, including experimental and FE modeling approaches, there are also predictive numerical methods based on thermal elastic-plastic, inherent strain, and inverse Eigenstrain methods. Smith and colleagues concluded that isotropic hardening models over-estimate the tensile welding residual stresses in stainless steel weldments. In contrast, pure kinematic hardening under-predicts the longitudinal stresses in parental material close to the weld. They then developed an optimized method based on isotropic-kinematic formulations to predict the residual welding stresses [189]. Javadi and teammates proposed combining FE simulations and ultrasonic stress measurement to nondestructively evaluate the welding longitudinal through-thickness residual stresses in stainless steel plates. The method was capable of investigating the top, bottom, and root of the main and back weld. In the HAZ, however, less agreement between FE and ultrasonic results were observed [128]. Until 2010, the study and simulation of welding procedures were primarily performed via either single-pass or 2D plane-strain and axis-symmetric models or 3D shell models [190]–[192]. Analytically, it is difficult to use a 2D model to study the effects of welding procedures such as deposition sequence or welding sequence on the final residual stress distribution. Significant progress in the field of computational welding mechanics was the implementation of 3D models. Deng [193] presented a computational approach to analyze residual welding stresses in a multi-pas joint, including a 3D model in which the effects of moving heat source, temperature-dependent thermal and mechanical properties, and annealing were taken into account. To characterize the through-thickness distribution of residual stresses as a function of welding heat input and geometry in stainless steel pipes. Two pieces of research in 2017 proposed a new data-based approach based on an artificial neural network (ANN) and verified the results with those of contour and neutron diffraction methods [194][195]. The ANN method successfully learned the non-linear patterns associated with residual stress fields in the HAZ and weld centerline.

Nevertheless, developing ANN models by constructing improved databases and performing a series of experiments to cover all regions of the process parameter space seems to be required in future studies. On the other hand, experimental methods are either destructive (i.e., contour and holed drilling) [183] or accompanied by uncertainties (i.e., XRD and neutron diffraction) [196].

Moreover, there are several limitations as well as simplifications in FE models [197]. In this case, further studies combined ANN, experimental, and FE analyses are suggested for future investigations in the field of residual welding stresses.

c) Spray Coating

Surface coating treatment is a feasible technique for achieving the desired mechanical and electrochemical characteristics of manufactured parts. Spraying powders, wires, or rods of preferred coating materials can produce a dense layer on the substrate surface, enhancing the fatigue performance and improving corrosion and wear resistance [198]. However, the development of undesirable residual stress during the process, particularly in thermal spray conditions, can deteriorate the coating's performance. Since the residual stress development can influence the coating adhesion and quality [199], bond strength, corrosion and wear resistance [200], and the fatigue life of coated materials [201]; hence, predicting, measuring, and controlling the residual stress developed by the coating process are crucial [202]. For this purpose, optimizing the processing parameters, selecting an appropriate coating material, and coating methods for customizing the induced stress are desirable.

Thermal spray techniques are extensively employed to protect and modify the structures in different industrial sectors such as automotive, aerospace, electronics, biomedical, power generation, petrochemical, and offshore. In all thermal spray methods, the powder or wire of coating materials is heated near or above their melting point by various power sources, including Plasma, Electric arc, Oxy-Fuel, and Oxy-gas Fuel combustion corresponding to different thermal spray techniques [203]. The molted particles are accelerated through the gas stream, impacting the substrate surface to create a coating layer with various thickness levels between 20 microns to several millimeters, depending on the feed rate, materials, processing parameters, and deposition methods. During the coating process and afterward, the residual stress can induce in the coating and substrate, which can be attributed to the peening of droplets, the rapid cooling and solidification of molted particles, and differences between the CTE of particles and substrate materials [204]. Moreover, during the thermal coating process, residual stress can be affected by some phenomena, including phase transformation, thermal gradient, and chemical reactions, which can even alter the sign of residual stress [201]. Therefore, developing detrimental (tensile) residual

stress in thermally sprayed materials is influenced mainly by the thermal phenomena and history, while the peening effect simultaneously induces beneficial (compressive) residual stress.

As a high-energy thermal source with a high-temperature deposition (12,000-16,000°C), the plasma spray technique is used chiefly for coating high-temperature materials, such as ceramics [201]. However, low particle velocity (150-400 m/s) and a high-temperature difference between particles and substrate lead to tensile residual stress, low coating density, phase transformation, coating delamination, and lower fatigue life [205][206]. Back et al. [207] reported the residual stress development in the MnCoFeO4 coating deposited on steel substrate by the plasma spray technique. They studied the effects of coating temperature and post-heat treatment on the induced phase transformations of the coating material, consequently, on the residual stress changes. Considerable tensile quenching stress and thermal stress were predicted because of the significant temperature differences between the substrate (200°C) and molten coating particles (1700°C), and CTE thermal mismatch during cooling. However, relatively low residual stresses were measured in the coating due to the stress relaxation during layer deposition; hence, in this case, thermal stress was predominant. On the other hand, the coated sample's heat treatment at 700°C for 10h resulted in increased residual stress due to the partial phase transformation of the deposited material and the pore density reduction. However, more extended heat treatment (100h) at 850°C decreased the residual stress level due to the phase transformation, residual stress relaxation, and a slight increase in porosity. In another research, an intermediate layer of oxide ceramic was deposited between NiCrAlY top coating and glass-ceramic substrate materials to decrease the detrimental effect of CTE thermal mismatch [208]. Moreover, they used compressed air cooling to minimize thermal stresses and reduce the cracking in the coating. Lasseur et al. [209] changed the printing strategy (planar and rotating patterns) to evaluate the residual stress induced in Zirconia coating on the steel alloy substrate during the plasma spray coating. They also examined the effect of grit-blasting and preheated substrate on residual stress development. The obtained results showed that grit-blasting with preheating decreased the compressive residual stress of the coating surface compared to the grit-blasting solely (Fig. 13(a)). Furthermore, the rotating pattern decreased the tensile quenching stress at the coating surface (Fig. 13(b)). In contrast, the planar pattern leads to the relaxation of more thermal stress in the substrate's depth because of the longer deposition time compared to the rotative pattern (Fig. 13(b)). Controversy results were obtained by Thakare et al. [210] when they used a stress relaxation technique to evaluate the residual stress in air plasma sprayed composite

coating (8YSZ-Alumina-MWCNT) on the P91 steel. In this research, preheating the substrate increased the compressive residual stress at the coating surface. Furthermore, increasing the percentage of alumina in the coating feedstock leads to an increase in the compressive residual stress of the surface; however, tensile residual stress was developed by adding the percentages of MWCNT due to its agglomeration. Pang et al. evaluated the aluminum alloy substrate preheating effect on the residual stress development during functionally gradient coatings of Mo/8YSZ using FE simulation. By employing a mathematical calculation, the radial and axial residual stress were determined separately. They found that the substrate's preheating decreased the redial tensile residual stress; however, it could increase the axial tensile residual stress [211].

In another thermal spray technique, High-Velocity Oxygen Fuel (HVOF), lower temperature deposition (2500-3200°C), and higher impact velocity (upper than 1000 m/s), leads to prevail the peening effect and induce the compressive residual stress. Zoei et al. [212] investigated the residual stress distribution of WC-10Co-4Cr coating on AISI 1010 steel deposited by the HVOF process. They measured compressive residual stresses being produced due to the peening stress and higher CTE of the substrate than the coating (mismatch stress) on the coating surface and the coating depth. Tensile residual stresses induced by quenching stress, however, had a minor effect compared to mismatch stress. The same observation was reported by Owoseni et al. [213] when they measured the residual stress of suspension HVOF sprayed Al_2O_3 coating on AISI 304 stainless steel substrate. Nevertheless, controversial results have been observed during the coating stellite-6 on steel substrate with the same spray process [214]. Developing tensile residual stress on the coating surface was reported due to the higher cooling stress and the lower peening stress at the coating surface. In contrast, the compressive residual stress was developed through the interior layer, interface, and substrate due to the higher peening and lower cooling stress [214]. In another research, the type N Almen strips and in-situ coating property sensors were employed to investigate the effects of quenching, peening, and cooling stresses on the formation of the residual stress in HVOF sprayed WC-10Co-4Cr coating. The in-situ measurements revealed tensile residual stress in the coating during the coating process due to the quenching stress. After deposition, the residual stress was altered from tensile to compressive due to the cooling stress [215].

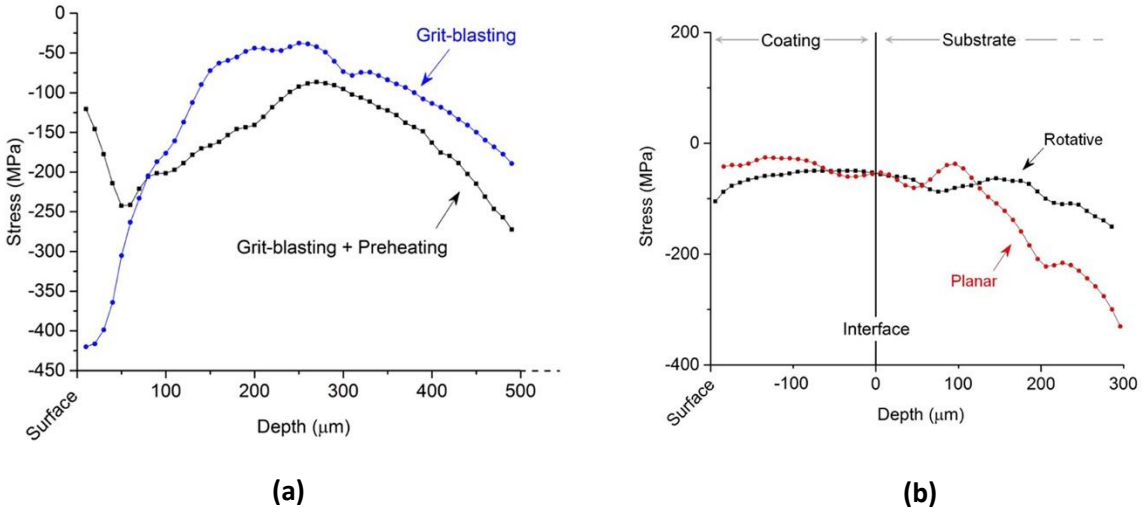

Fig. 13: a) Residual stress distribution for grit blasted substrate (Feed rate 20, the pressure of 2 bar), with and without preheating at 300°C; b) Residual stress distribution for grit blasted (Feed rate 20, Pressure of 2 bar), preheated at 400°C and YSZ coated at 300°C in rotative and planar patterns. Adapted with permission from reference [209]. Copyright 2020, Springer.

Cold gas dynamic spraying as a solid-state material deposition is another feasible coating technique used to print a wide range of materials. In this process, the residual stress distribution is more affected by the peening stress and plastic deformation of particles instead of the thermal phenomena due to the nature of this technique [216]. Unlike thermal spray methods, in cold spray, coating layers are formed as a result of the high kinetic energy of particles impact rather than the liquid phase material joining. The kinetic energy is provided by accelerating micron-size particles of coating material supersonically towards the substrate surface through a relatively low carrier gas temperature (far from the melting point of coating material) [217]. Considerable benefits, such as oxidation-free surface, no phase transformation, high coating density, and compressive residual stress development in coating and substrate, have been claimed to be achievable by cold spray coating. However, despite the inherent characteristic of cold spray offering beneficial residual stress, stress relaxation, or even tensile residual stress was reported in the coated materials. The temperature of carrier gas, heat generation during particles' impact, and differences between CTE of substrate and coating during the cooling are significant sources for altering the peening stress in coated samples. Also, the induced stress can be influenced by the processing parameters (carrier gas temperature and pressure, nozzle travel speed, feed rate), substrate surface roughness, and

coating thickness [218][219]. Different approaches were employed to reduce the detrimental effects of residual stress on cold sprayed materials, particularly for thermal-sensitive materials.

Bhowmik et al. [220] investigated the effect of post heat treatment on the residual stress induced in the cold sprayed Ti–6Al–4V coating on the Ti–6Al–4V substrate. They found that the tensile residual stress developed at the coating surface for as-sprayed samples was relieved after heat treatment and altered to compressive stress. Moridi et al. [221] studied the effects of pre-and post-shot peening treatment on the residual stress distribution in cold sprayed materials. They claimed that pre-shot peening increased the depth of inducing compressive residual stress in the Al6082/Al6082 coated samples compared to the post-shot peening treatment. Another post-treatment technique, Friction-stir processing, was employed in independent research to modify the surface of cold sprayed Ti coating on Al5083 substrate [222][223]. Khodabakhshi et al. evaluated the residual stress development of coated samples before and after post-treatment processing. The reported results showed a considerable amount of compressive residual stress developed on the coating surface after employing the high plunge depth friction-stir process on the cold spray coated samples [223]. In another research, Vargas-Uscategui and teammates studied the role of some processing parameters, such as nozzle travel speed and powder feed rate on the residual stress distribution in cold spray additively manufacturing hollow titanium cylinders. The measured residual stress using a neutron diffractometer revealed tensile residual stresses near the cylinder walls' inner and outer surfaces, while compressive residual stress was induced in the wall center. Inducing tensile residual stress can be attributed to the thermal effect, mainly when the nozzle speed was low. Moreover, increasing the powder feed rate caused an increase in the residual stress. On the other hand, the peening effect was predominant for the higher nozzle travel speed [224]. As a general guideline, increasing the nozzle's speed reduces the heat input during the process, decreasing the thermal effect, promoting the compressive residual stress. Nevertheless, in low melting point and temperature-sensitive materials, such as magnesium and zinc alloys, cold spraying is warm enough to provide sufficient thermal energy for changing the state of stress in competition with the peening effect. In this case, reducing the heat input might be insufficient to eliminate the coating temperature effect and promote the peening effect towards developing the compressive residual stress in the deposited material and substrate, especially near the interface. In this situation, engineering the heat balance would be an effective strategy to control the residual stress. Recently, Marzbanrad et al. [219][225] investigated the effect of processing parameters,

including temperature and pressure of carrier gas and nozzle travel speed on the residual stress distribution in the cold sprayed Al7075 coating on the AZ31B magnesium substrate. They demonstrated that the temperature of the carrier gas has the most significant effect on the residual stress compared to the other parameters. However, for creating a high-quality coating with a good bond strength, a minimum temperature of carrier gas is required to provide the desired particle velocity upon impact. Therefore, the carrier gas temperature was kept constant at the minimum acceptable value. The heat input and heat transfer were controlled by increasing the nozzle travel speed and accommodating a water-cooled heat sink under the substrate [202]. Residual stress measurements revealed that significant compressive residual stress was successfully developed at the coating surface, interface, and substrate near the interface (Fig. 14). At the same time, the physical and mechanical characteristics, as well as the microstructure of coated material, were improved [225]. In addition, to reduce the detrimental effect of CTE on the residual stress, Marzbanrad et al. [226][227] coated zinc as an intermediate layer between Al7075 top coating and AZ31B substrate. The use of zinc with higher CTE than magnesium and aluminum alloys reduced the thermal mismatch effect and controlled the residual stress in this multi-layer system.

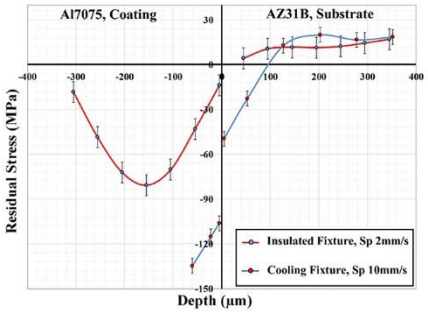

Fig. 14: Residual stress profile for cold spray coating Al7075 on AZ31B with changing the heat balance. Adapted with permission from reference [225]. Copyright 2021, Elsevier.

3.1.2. Mechanical

a) Machining

Residual stresses generated during machining can be seen as a decisive factor in identifying fatigue life and surface integrity in machined workpieces. Besides, residual stress impacts the distortion and quality and wear and corrosion resistance of the machined specimen. A report in 2001 indicated that it cost Boeing company approximately 290B USD to compensate for the distortion

in machined components [228]. This underscores that residual stress distribution patterns should be accurately identified in the machining process. The research has shown that machined components with compressive residual stress would have longer fatigue life than unmachined raw components. On the other hand, tensile residual stress appears to help fatigue crack growing and shorten the component fatigue life. Residual stress in the machining of thin-walled parts induces workpiece distortion and dimensional instability [229]. Amini et al. [230] investigated the residual stress in machining high-strength thin-walled aluminum alloys and indicated machining force, and temperature directly correlate with residual stress. Heat treatment can induce residual stress in the workpieces; accordingly, machining these parts leads to more distortion and production scrapes [231].

It has been established that the residual stress induced through wire electrical discharge machining (WEDM) is negligible at the millimeter scale. Nevertheless, on the condition that the dimensions of the machined product are less than a few millimeters, the structural modification of the EDM layer might play a crucial role in altering its structural integrity through microstructural changes and induced residual stresses. The residual stress response due to WEDM cutting is well discussed in [232].

Over recent decades, various destructive and non-destructive methods aimed at measuring machining-induced surface and internal residual stress have been developed. Moharrami et al. [96] utilized the ring-core method to measure residual stress in milling of narrow circular grooves in which the error value was lower than 1.5%. Chupakhin et al. used the hole-drilling method to study the effect of material behavior on residual stress profile determination [233]. Azhiri et al. [234] studied the residual surface stress in the ultrasonic-assisted electrical discharge machining process. They used the XRD technique, finding out that the presence of ultrasonic vibration helps to reduce surface tensile residual stresses due to the peening effect on the workpiece surface.

Scholars have widely examined the influence of different factors on the residual stresses in the machining process. Implementing the Taguchi orthogonal array together with high-speed milling of gamma titanium aluminide pointed out that machining parameters, including cutting speed, feed rate, axial and radial depth of cut, workpiece angle, flank wear, and milling direction, would highly influence residual stress profile [235]. As demonstrated by Fig. 15, cutting speed and flank wear have the most significant effect on residual stresses value.

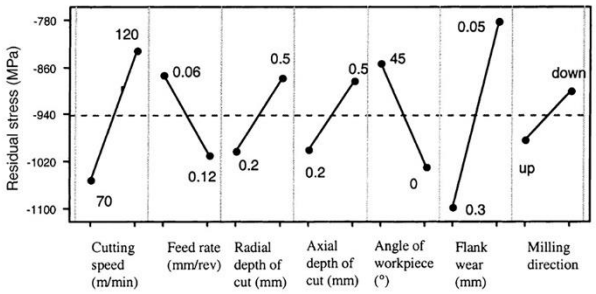

Fig. 15: The influence of different parameters on the residual stresses in high-speed milling. Adapted with permission from reference [235]. Copyright 2001, Elsevier.

Dahlman et al. [236] investigated the tool geometry and chipping parameters effect on the residual stress during hard turning of AISI 52100, perceiving that negative rake angle and larger feed rate induce compressive stress. Also, the increment of rake angle moves compressive residual stress deeper into the material, and depth of cut is not a significant parameter on residual stress. They declared that compressive residual stress always occurs beneath the surface. The effect of coolant usage in face milling of age-hardened Inconel 718 was investigated in [237]. Using coolant in face milling with Carbon Boron Nitride (CBN) inserts results in compressive residual stress or lower tensile residual stress. Insert geometry was also discussed. Square inserts generate tensile residual stresses while rounded inserts generate compressive ones. The authors suggested that the milling operation with rounded inserts in lower cutting depth and cutting speed using coolant tends to generate lower surface roughness and residual stresses. In another research, Meng et al. [238] studied tool nose radius and tool wear influences on the residual stresses during hard turning of bearing steel. Three CBN tools were used in three different tool nose radiuses. Performing XRD and electropolishing, they declared that tool nose radius is the most significant parameter in residual stress distribution, which is due to the plowing effect of the tool that causes an increment in magnitude and depth of residual stress. This is in accordance with other investigations [239][240]. A worn tool would also shift residual surface stress to tensile stress and increases subsurface compressive residual stress. Tang et al. [241] examined the tool wear influence on the residual stresses in milling of 7050-T7451 aluminum and obtained the same results as [238]. Li et al. stated that cutting force is the most significant factor associated with machining-induced residual stresses. Compressive residual stress quantity is directly related to machining cutting force [242].

Overall, the higher quality of specimen surface requires compressive residual stress. In machining operations, compressive and tensile residual stresses are the consequences of mechanical and thermal loads, respectively (Fig. 16) [243].

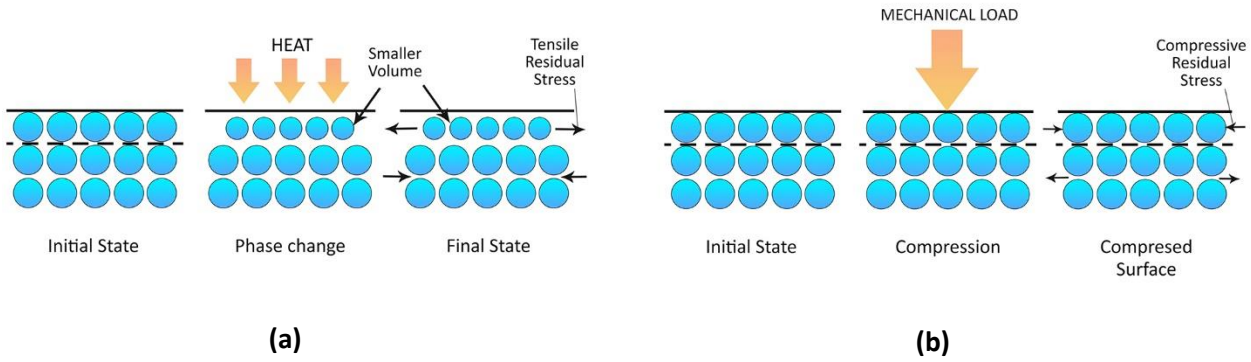

Fig. 16: Creation of residual stresses as a result of a) thermal and b) mechanical loads. Adapted with permission from reference [243]. Copyright 2006, Elsevier.

Rao et al. [244] showed that more considerable compressive residual stress results in better surface quality. They proved that in high-speed milling of 7075-T6 aluminum, secondary cutting edge rubs the surface, reduces temperature, and prevents built-up edge generation because of intermittent tool-workpiece contact. Lower thermal load on the specimen surface causes colder plastic deformation that leads to compressive residual stress generation. The influences of thermal properties associated with the workpieces were also investigated [245]. A higher thermal softening exponent and thermal conductivity would cause more significant tensile residual stresses near the workpiece surface. In contrast, the thermal softening exponent has a higher impact on machining-induced residual stresses.

Composites usage is rising in different industrial zones, including aerospace, medical engineering, and civil engineering, in recent decades [246][247]. Because of having multiple materials with various properties, residual stress examination is complex and needs to be investigated more deeply in these materials. Pramanik et al. [248] conducted a deep examination on the effects of ceramic reinforced particles on residual stress in turning aluminum alloy. Machining-induced residual

stress in the non-reinforced aluminum alloy was tensile and increased by feed and speed increments. On the other hand, after being reinforced by ceramic particles, compressive residual stress was generated and decreased by feed increment. Moreover, the speed effect on the residual stress is insignificant. Lin et al. [249] studied residual stress in the turning operation of TiB_2/7050 Al metal matrix composite. It was obtained that the presence of TiB_2 particles helps to the creation of compressive residual stresses. Moreover, the largest compressive residual stress occurs while using new tools that are not worn. Tool wear appears to induce compressive residual stresses in deeper areas compared to the surface of the specimens.

Many researchers have tried to predict residual stress before machining and proposed empirical and analytical models in this regard. Empirical models are often acceptable in a certain range of the machining parameters. The established models are also used to conduct residual stress optimization. Capello et al. [250][251] established a regression model to examine the influence of turning process parameters on the residual stresses. The proposed model encompassed combination of process parameters and machined material properties. Therefore, for carbon steel and alloyed steel, separated models were established. The error rate was observed to be approximately 5%. Sharma et al. [252] constructed a statistical residual stress model in ultrasonic-assisted turning operation of 4340 hardened steel. Analysis of variance was also carried out in which a good agreement between experimental and predicted values with a 95% confidence interval was achieved. Besides, the optimized condition was found to be in cutting speed of 30 m/min, a feed rate of 0.1 mm/rev in the presence of ultrasonic vibration with an intensity of 60%, resulting in compressive residual stress.

Moreover, in recent decades, machine learning methods were utilized to either establish a predictive model or optimize the process parameters to minimize residual stress. Zhang et al. [253] utilized two methods to predict residual stress in finish hard turning of two materials with various process parameters, namely “linear regression model” and “intelligent empirical model” of back-propagation neural network. Intelligent way resulted in lower than 10% error value while that of the regression model was over than 100% in prediction of the circumferential residual stress profile. Employing the genetic algorithm, Jafarian et al. [254] conducted multi-objective residual stress and surface roughness optimization. They declared that there was a good agreement between the experimental and obtained optimal results. Residual stresses can be predicted analytically by

knowing the cutting temperature and mechanical loading history [255]. Liu et al. [256] proposed an analytical model for predicting the residual stress distribution and depth of plastic deformation in the ultrasonic-assisted single ball burnishing process. The accuracy of the residual stress predictive model in the worst case was less than 20% which was acceptable compared to other predictive models [257][258]. The effects of the process parameters on the residual stress distribution in the predictive model were seen to be in good accordance with other research works [259][260].

Numerical simulation is arguably the primary technique to predict residual stresses more realistically. By numerical simulation, machining-associated costs can be saved and, the process parameters will be controlled and optimized, which, in turn, could minimize the unwanted residual stresses. Wei et al. [261] compared experimental and numerical machining-induced deflection of thin-walled aerospace parts due to residual stress. They stated that if the length of the workpiece were much longer than the width, the impact of the longitudinal residual stress on the distortion would be more prominent compared to the lateral one. Jafarian et al. [262] carried out a 3D numerical study on dry machining of Inconel 718 alloy and achieved a good agreement between experimental and 3D numerical outcomes. Pan et al. [263] proposed a microstructural-based FE simulation to examine surface residual stress in 2D orthogonal turning. The simulated section was verified by experiments in different feed rates and cutting velocities.

b) Additive Manufacturing

A tremendous amount of residual stresses is produced in different additive manufacturing processes such as selected laser melting (SLM) [264][265], wire arc additive manufacturing (WAAM) [266]–[268], and laser powder bed fusion (LPBF) [269]–[271]. Given the high volume of publications related to the measurement and mitigation of residual stresses in different additive manufacturing processes, this area will require a specific investigation and not be discussed in this paper. An excellent review on this topic has recently been published [272].

3.2. Effects:

3.2.1. Fatigue, Fracture and Structural Integrity

a) Engineering Sciences

This section represents the fatigue/fracture performance of engineering materials considering the residual stress state, covering different areas such as manufacturing and welding procedures. As pointed out by Prime [273], there is a two-way relationship between residual stresses and fatigue/fracture, meaning that residual stresses might add to applied loads, contributing to failure processes such as fatigue and fracture, and, on the other hand, fracture mechanics can immensely contribute in residual stress assessment by simplifying calculations using the superposition principle. Research by Hosseinzadeh and teammates explains that in the contour method, the second most crucial factor affecting the accuracy of stress measurements is control of plasticity during a contour cut, which could be achieved by applying fracture mechanics concepts, that is, by minimizing the stress concentration at the tip of the wire electric discharge machining (WEDM) cut [274].

The relative importance of residual stress and fatigue/fracture can be explained by the concept of mode I stress intensity factor (K_1) used for fatigue and fracture as follows:

$$(K_1)_{applied} + (K_1)_{rs} > K_{1c} \quad (2)$$

In which $(K_1)_{rs}$ denotes residual stress contribution to stress intensity factor (K_1). This equation well illustrates that the contribution of residual stresses in the failure process can be either beneficial provided that $(K_1)_{rs}$ has negative values (compressive stresses) or harmful for positive values of $(K_1)_{rs}$ (tensile stresses). It also turns out that residual stresses would have a more powerful impact on fatigue crack growth than high-cycle fatigue [273]. Prime and teammates tested a new experimental, forensic approach on a large 7000 series aluminum alloy that had fractured under brittle conditions, analyzing the residual stresses that had contributed to mode I fracture. This method was verified to be applied to map residual stresses immediately before brittle fracture, even if the original crack grew due to stress corrosion or fatigue cracking [275]. Another exciting work regarding the intersection of residual stress analysis and linear elastic fracture mechanics was presented in 2016 by Ribeiro and Hill, where a solution, taking into account residual stress fields and stress intensity factor as a function of crack size, for a 2D Eigenstrain problem was developed [276]. Performing the XRD method, Appel et al. investigated the role of residual stresses in fracture toughness behavior of TiAl alloys [277]. A very recent study by Salvati [278] combined the Phase-Field method and the eigenstrain theory to study the influence of residual stress on the fracture

toughness of brittle materials, concluding that residual stress can be thought of as a toughening mechanism to attain unprecedented material or structure performance.

The influence of compressive residual stresses on the fracture toughness of dental glass-ceramics (GCs) was studied in detail in [279]. This work, however, did not investigate the tensile residual stresses in GCs.

Different residual stress/fatigue research papers also verify that the changes (relaxation or increase) in residual stresses under uniaxial or thermal cyclic fatigue loadings primarily happen during initial cycles [166][280]. In other words, as shown in work by Tabatabaeian et al. [42], the influence of initial cycles are more significant than the rest of the cycles, which means one can examine the stress response of materials exposed to particular cyclic fatigue conditions by analyzing only a limited number of early cycles. There is a large body of research associated with the fatigue life of materials in the manufacturing process, focusing on residual stress quality. In 2013, Kim et al. [280] presented a fatigue limit criterion based on the critical threshold residual stress relaxation concept for shot-peened carbon steel specimens. Ref. [281] clearly shows that depending on the magnitude and direction of residual stresses, fatigue crack propagation behavior in additively manufactured (AM) engineering components might be affected significantly. Based on the outcomes of [282], residual stresses play the dominant role in improving the fatigue life of plasma electrolytic oxidation coated (PEO) Ti-6Al-4V alloys. This alloy is also widely used in other AM procedures such as selected laser melting (SLM), where complex thermal gradients and localized melting and solidification phenomena cause process-induced residual stresses. The findings of research in 2019 suggested that residual stresses are a significant factor concerning the fatigue crack behavior of SLM Ti-6Al-4V. It is recommended that if a ‘tall’ part geometry is required, a stress-relief heat treatment is considered to minimize residual stresses and enhance fatigue crack growth performance [283]. Another recently published paper reveals significant 88% improvement in fatigue life of components can be achieved by introducing localized compressive residual stresses at critical zones [284].

In addition to manufacturing processes, it turns out that fatigue crack propagation during the welding process could also be influenced by the residual stresses [285]. Research on the fatigue life of the welded steel structures shows that fatigue crack growth behavior in welded offshore structures, particularly near the threshold region, highly depends on the residual stress state [286].

On the contrary, Tra et al. reported that even though remarkable amounts of residual stresses are generated during the welding operations of aluminum alloys, they had a minor effect on the fatigue crack propagation behavior, especially in friction stir welding processes. A very recent study in this circle highlights the importance of quantifying and removing coupon residual stresses while fatigue crack growth rates are measured in the welded pipelines [287]. Contradictory outcomes in this field suggest that further investigations regarding the influence of residual stresses on the fatigue performance of welded structures are required. It may be of interest for future studies to precisely classify different welding techniques and the role of residual stresses on the fatigue crack propagation as well. Goswami et al. [288] studied the changes in residual stresses around the fatigue crack in two different aluminum alloys, observing that residual stresses around the fatigue crack increase by 200% for Al 7075 while decrease by 80% for Al 1100. These results arguably suggest that in addition to changes in dislocation density for both alloys, there is another major factor affecting residual stresses, which is the deformations associated with lattice rotation. This paper provided new insights into the key role of lattice rotation in determining residual stresses around the fatigue crack area. A numerical study regarding the influence of initial residual stresses on the rolling contact fatigue life of wind turbine carburized gears revealed that these initial stresses do not affect the amplitude of stress and strain but influence the maximum and mean values. This research also employed and compared two multiaxial fatigue criteria, namely 'Fatemi-Socie' and 'Brown-Miler'. Based on the former, residual stress affects contact fatigue damage through its maximum normal stress. The results obtained from the latter criterion suggest that for compressive residual stresses higher than a specific value, the rolling contact fatigue damage will not experience any increase [289]. Gu et al. proposed a microstructure-based model to study the influence of residual stresses on the fatigue crack initiation behavior of martensitic steels. The findings well underscored the necessity to take into account residual stresses for future fatigue modeling and assessment [290].

b) Medical Sciences

In addition to the world of engineering, residual stresses are vastly studied in medical and dental disciplines. Residual stresses and strains have a vital role in the mechanical function of biological systems, such as veins, arteries, stomach, brain, intestine, cartilage, skin, and teeth [43, 276, 277]. A concrete example of this can be seen in blood pressure, where compressive residual strains

increase as blood pressure gets higher. It is, therefore, worthwhile studying the interaction between residual stresses and different biological structures.

In bone structure, residual stresses may exist at multiple length scales, from micro-scale residual stresses in collagen fibrillar structures to the macro-scale stresses associated with whole bone growth. Given the significant contribution of residual stresses in bone strength and bone adaption, it is interesting to understand the residual stress quality in bone tissue [293]. It is turned out that when the bone is cut into smaller pieces, macro residual stresses are released. A key experimental technique to characterize the residual stresses in the bone constituents is X-ray scattering. Findings of research in 2017 signify that contour and hole drilling methods can qualitatively determine differing stress states and expected stress profiles in biomedical implant castings, while XRD is a feasible quantitative technique. Moreover, neutron diffraction is not a feasible method to determine residual stresses in implant castings [294]. Tung et al. implemented XRD to quantitively determine the influence of hydration and X-ray radiation dose on the residual stress states of the cortical bone constituents. It was clarified that water content would considerably affect the residual stress of the collagen structure in bone [295].

A review of recent investigations highlights the preponderant role of residual stresses in the failure of ceramic and composite dental materials [296]. These stresses could be generated due to mismatch in CTE and tempering or grain anisotropy, amplifying the cycling stress profile in the oral environment and initiating cracks in areas with preexisting tensile stress. On the other hand, surface treatment techniques such as sandblasting can cause beneficial compressive residual stresses, contributing to adhesion enhancement in dental crowns [297].

Porcelain-veneered zirconia (PVZ) is a popular choice for crown restorations. The veneer layer of these dental restorations, nevertheless, is prone to delamination results from the development of residual stresses during the cooling phase of veneer firing. XRD characterization of residual stresses in the zirconia core of dental crown systems provided profound insights into residual stress profiles in zirconia. The magnitude of residual stresses was seen as large as 1 GPa locally, increasing after veneering with porcelain [298][299]. The XRD, however, cannot give the same information in the amorphous porcelain layer. The hole-drilling method is also challenging if there are limited locations in which drilling can be performed [300]. In an attempt by Zhang and Hanan in 2011, a new method to characterize residual stresses in dental crowns, called nanoindentation,

was proposed and then modified in 2012 [298]. The results showed that geometry and thickness would have considerable effects on residual stresses across dental crowns. Research findings in 2015 signify that residual stresses in metal-ceramic dental restorations can be reduced by 10% and 20% by changing interface configuration from conventional sharp transition to 50% metal-50% ceramic interlayer and using functionally graded material (FGM) interlayer, respectively [301]. An experimental investigation on the residual stress distribution in dental materials by Wendler et al. [302] suggested that cooling rate has a negligible effect on residual stresses but a significant role in hoop stress development, clarifying the fact that interaction between stress components appears to govern stress distribution and multiaxial assessment in three-dimensional structures is required for a thorough analysis of residual stress distribution. Accomplishing nanoindentation in fractured or suspended fatigued 3-unit fixed dental prostheses, Fardin et al. observed that the highest concentration of residual stresses exists within the outer layer of the porcelain veneer, and these stresses drop towards the framework/veneer interface [303]. Sebastiani et al. used the FIB-DIC ring core measurement method along with scanning electron microscope (SEM) imaging, and a direct correlation between residual stress distribution and fracture toughness in heat-pressed ceramic on zirconia core was proposed [86].

According to [304], residual stresses predicted via the viscoelastic finite element method (VFEM) are in better agreement with experimental measurements than those of the linear elastic finite element method (LEFEM). Dhital et al. [305] presented a VFEM analysis of residual stresses in PVZ, pointing out the importance of elastic modulus, coefficient of thermal contraction (CTC), and thickness ratio on the residual stresses developed in dental crowns. As concluded in [306][307], compressive residual stresses are commonly known to be beneficial due to their contribution to crack reduction and increased bending strength, and fatigue life. The nature of stress development is, however, complex and the long-accepted notion that compressive residual stresses created in the veneer are positive is an over-simplification that ignores the influence of geometry, thermal history, and material properties on stress development [300]. Therefore, it is suggested for future studies in this field to take various influential parameters into account while analyzing residual stress development in dental materials.

4. Control Methods

As presented in previous sections, residual stresses are often generated inevitably during different manufacturing and in-service stages of various materials, including metals, ceramics, polymers, and their composites, leading to warping, cracking, delamination, and reduction of fracture toughness and fatigue life. This is, therefore, of great importance to explore new methods by which these stresses can be controlled. Research papers in this realm introduce several strategies for optimizing residual stresses, ranging from manufacturing conditions to thermo-chemo-mechanical treatments. This section is organized based on the materials as follows:

4.1. Laminated Composites

4.1.1. Curing Process

To reduce residual thermal stresses in CFRP composites, Kim et al. devised a cure monitoring system using dielectrometry and a fiber Bragg grating (FBG). The revised cure cycle decreased residual thermal strains by 48.6%, while the flexural strength also decreased by 20.6% [308]. Fernandez et al. explored thermal treatments at different temperatures and times to control tensile residual stresses in metal matrix composites. Their findings revealed that it is possible to greatly control tensile residual stresses below a specific treatment temperature while increasing the yield strength [309].

4.1.2. Nano Additives

Significant progress in the reduction of unwanted thermal residual stresses in polymer composites was made by Shokrieh et al. [103][310], where they added different percentages of carbon nanofibers (CNFs) to the epoxy matrix, observing that the CTE of matrix highly decreases with CNF addition, while Young's modulus increases moderately. These outcomes confirmed that nanoparticles have good potential to control residual stresses and modify the thermo-mechanical behavior of the epoxy matrix. This was then tested and extended for CFRP and GFRP structures as well. Ghasemi and teammates [166][311][312] accomplished slitting and hole drilling techniques to measure the residual stresses in GFRP and CFRP composites with (1%) and without (0%) nanoparticles, concluding that the addition of an appropriate content of nanoparticles could be an effective way to reduce residual thermal stresses. This can be attributed to a large interfacial area between the nano-additives and the matrix, a strong interface bonding, and a good impregnation of the nano-additives with the matrix. In a recent study by Jafarpour et al. [313], the influence of different

distribution patterns of CNFs on the residual stresses of CFRP and GFRP composites was numerically examined and compared with experimental results (Fig. 17).

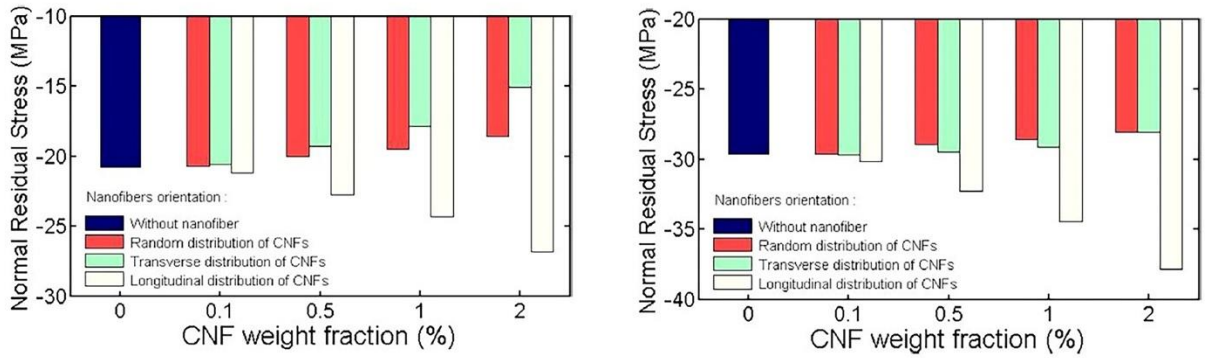

Fig. 17: Normal residual stresses in $[0/90]_s$ nanocomposites with different CNF orientation: a) GFRP, b) CFRP. Adapted with permission from reference [313]. Copyright 2019, Elsevier.

As shown by Fig. 17, adding CNFs with random and transverse distribution leads to reduced residual stresses. The longitudinal distribution of CNFs, nevertheless, appears to increase stresses. It is also clarified that the addition and orientation of CNFs would significantly influence the residual stresses of GFRPs compared to CFRPs.

4.2. Metals

4.2.1. Metals Welding

Several papers have provided methods to control residual welding stresses, including mechanical and thermal tensioning methods. In the former, a sufficient load, which can generate compressive residual stresses along the weld line, is applied proposedly. This appears to have a considerable influence on the reduction of destructive tensile residual stresses. On the other hand, mechanical tensioning techniques might suffer from some practical limitations; for example, they can only be applied to linear welds and are not viable when huge loads are required. The latter includes either the cooling or heating process during the welding operations. In this case, the thermal stresses are generated to either prevent the formation or reverse the misfits associated with the welding procedure [314]. Experience has shown that for some sensitive materials such as aluminum alloys,

cooling would be a better option, which can be performed locally or globally. Research findings reveal that a reduction of nearly 48% in residual welding stresses can be achieved by the multi-electron beam heating method [315]. Ramjaun et al. recommended that low transformation temperature (LTT) filler alloys have the potential to induce compressive residual stresses in the weld metal of both single and multipass welds, thus mitigating residual welding stresses to some extent [176]. In fact, by engineering the phase transformation temperature of the weld metal to take advantage of transformation expansion, the residual stress state within the weld zone can be significantly altered. A detailed review study regarding the design and application of LTT weld fillers to overcome tensile residual stresses in the welding process can be found in [316]. In 2017, Moat and teammates developed this method, proposing a carefully selected elevated inter-pass hold temperature to restore the LTT capability to achieve better residual tensile stress mitigation [317].

4.2.2. Metals Manufacturing

Another crucial area associated with controlling residual stresses is the manufacturing procedure of metallic materials [318]. An effective way to mitigate residual stress quality in the manufacturing stage is to introduce mechanical surface treatments such as shot peening, deep-rolling, and ultrasonic nanocrystal surface modification (UNSM). These surface treatment approaches induce compressive residual stresses, helping to delay crack initiation caused by tensile residual stresses so that fatigue resistance will improve to some extent [319][320]. Wu et al. investigated the influence of shot peening coverage on the residual stress of 18CrNiMo7-6 rollers, providing an advisory reference for the optimization design of shot peening parameters to control residual stress profile efficiently. Their findings revealed that increasing coverage does not appear to significantly improve the residual stress level once the full coverage condition is achieved [321]. Aiming at reducing residual stresses generated by micro-grinding, which is a particular machining method [322], Ding and teammates thoroughly studied the phase transition process, developing a constitutive model. The results highlighted the necessity of selecting a medium linear speed of the grinding wheel, a significant feed rate, and a small grinding depth. The phase transitions could be controlled to promote the transition of ferrite to austenite could further reduce the residual stress [323]. Yang et al. represented a FE simulation model to study the quench residual stresses of

aluminum alloy. The maximum tensile and compressive residual stress of the quenched cylindrical bar decreased with increasing water temperature [324]. Research by Ahmed et al. [325] suggests that depending on the deposition efficiency, the residual stress arises from electrical discharge coating (EDC) process can be controlled or reduced by alternating parameter sets.

Another emerging method that can be applied for residual stress relaxation, is vibratory stress relief (VSR) process, which is a general stress relieving method via cyclic loadings caused by vibration. Compared with heat treatment, the VSR method has such advantages as low cost, a short process time, small-volume equipment requirements, and slight energy consumption. However, this method is confined to large pieces [326][327]. Gao et al. [328] studied the influence of the VSR on the fatigue performance of 7075-T651 aluminium alloy. Another research by authors [329] compared thermal-vibratory stress relief (TVSR), thermal stress relief (TSR), and vibratory stress relief (VSR), concluding that the TVSR can effectively reduce the residual stress in 7075 aluminum alloy, and the stress relief rate of TVSR for the peak stress are 20.43%, and 38.56% higher than that of TSR and VSR.

Successful transition from rapid prototyping to additive manufacturing (AM) is an exciting challenge that requires careful control of the integrity of the parts to be put in service. A significant risk for additively manufactured parts is the build-up of residual stress. In this case, control of residual stresses emerging in metals and alloys during different manufacturing processes is another critical area covered in this section. Current approaches to reducing undesired residual stresses in AM processes include (1) altering the scanning strategy [330] or (2) heating the build plate [331]. Vastola and teammates presented an experimentally validated FEM model to assess the impact of different parameters on the control of residual stresses during the AM process of Ti6Al4V. It was found that the bed preheating temperature would have the largest quantitative impact on the residual stress, with lower stresses recorded at higher bed temperatures [332]. Also, the results of research in 2017 signify that increasing the bed temperature to 570 ℃ highly reduced residual stress formation within components manufactured by the SLM process [333]. Roehling et al. succeeded in reducing residual stresses up to 90% in 316L stainless steel bridges manufactured by the laser powder bed fusion (LPBF). This was performed by controlling the surface temperature of the material in-situ, while no stress-relieving post-processing was required. Further developments regarding controlling residual stresses in the LPBF process could be made by

optimizing the frequency of the in-situ diode annealing process (i.e., number of layers per heating cycle) [334]. More information regarding the formation, prevention, and control of residual stresses in metal additive manufacturing can be found in a recently published review article by Carpenter and Tabei [272].

5. Conclusions and Perspectives

The importance of residual stress within the broad field of engineering materials is demonstrated by the fact that it is now a prominent area of research. In this paper, an updated review of the recent progress associated with the field of residual stress is presented. The paper is classified into three main sections, including “determination methods”, “origins and effects” and “control methods”.

It is clarified that determination methods could be fell into either experimental measurements or analytical studies. Among the experimental methods, the contour, hole drilling, and slitting methods have seen the most significant developments over the recent decade. Also, applications of non-destructive neutron and X-ray diffraction methods in different engineering procedures are covered in detail. Apart from these experimental techniques, analytical and numerical methods characterize residual stresses in a time-effective and low-cost way. The main drawback associated with the analytical and FE predictive models is that they cannot fully consider all the real-life conditions, such as unexpected changes in environmental, mechanical, or thermo-chemical features, which can cause errors in predictions. On the other hand, all experimental measurement techniques have their limitations and sources of uncertainty. Even if these shortcomings did not exist, it would still not be possible to carry out through-thickness non-destructive measurements in-situ on the components with heterogeneous microstructures and complex geometries. In this case, the sensible idea is to quantify the residual stresses through numerical modeling, with selective measurements being carried out to validate the model that has been employed. It was observed that the attention has recently moved to artificial intelligence (AI) analysis, trained using the experimental tests. Accordingly, experimental techniques appear to have the most significant impact on future works, given their precision and the opportunities they potentially have in AI algorithms training and verification of predictive analytical and numerical models. Moreover, developed three-dimensional FE models and theories considering more real-life conditions seem to be required. Given the current trend, more prospects are seen for the slitting method to take the lead among experimental techniques; however, contour and hole drilling are the most practical

ones currently used, and as profoundly discussed earlier, novel methods, including replacing strain gauges with SHM techniques, optimizing the cutting or drilling strategies and reduction of calibration coefficients are emerging. Moreover, mechanochromic and non-contacting optical approaches hold considerable promise to detect residual stresses in engineering materials. It is expected that if the current trends in AI studies, self-sensing materials, and non-contacting optical methods such as DIC are set to continue, a significant breakthrough in the field of residual stress monitoring will be made soon.

A review of various science areas dealing with residual stress indicated the significant impact of residual stresses on corrosion, fatigue, welding, machining, spray coating, dental materials, etc. Therefore, an optimized design of residual stresses can significantly extend the fatigue lifetime and durability of the engineering products. An essential yet less focused point perceived from some contradictory results in the literature presented in this paper is that due to the complexity of microstructure changes and interactions between different phases in micro-scale, prediction of residual stresses would be challenging. For example, it was seen that even though compressive residual stresses can be constructive in different engineering applications, they are sometimes likely to have detrimental effects on dental materials, as discussed in section 3, Also, it was observed in section 2 that different measurement methods could have different results under particular conditions. In this regard, a thorough case study for any given process that might induce residual stress appears to be crucial. In addition to the six main areas covered in ‘origins and effects’ section, residual stresses are significantly produced in different additive manufacturing processes such as SLM, WAAM, and LPBF. Given the ever-increasing use of AM technologies, a part of future studies should be allocated to residual stress monitoring in additive manufacturing technologies.

Finally, several methods to control and reduce residual stresses in different engineering materials were reviewed and discussed in the last section. It was shown that residual stresses could be well controlled via various methods, such as adding an appropriate content of nanoparticles, optimizing the curing/cooling cycles, and conducting heat treatment and surface treatment methods such as PWHT, shot peening, and WNSM. Besides, the progress in manufacturing techniques can help to reduce unwanted process-induced residual stresses. It was also reported that either of these strategies might have unpredicted results. For example, the addition of nanoparticles may induce

detrimental tensile residual stresses due to agglomeration effects. If not properly implemented, the heat treatment after the welding procedure has been reported to bring about undesirable microstructural changes. These examples confirm that methods to mitigate residual stresses would work under an optimized situation. In this case, more insights into nano additives that can induce or reduce compressive/residual stresses at any given area of the components are also of interest for future works.

Authorship Contribution Statement

Ali Tabatabaeian: Conceived of the presented idea, References, and resources, Writing- original draft, Writing- review & editing.

Ahmad Reza Ghasemi: Writing- review & editing, Supervision- providing critical feedback.

Mahmood M. Shokrieh: Writing- review & editing, Supervision- providing critical feedback.

Bahareh Marzbanrad: Writing- The "Spray coating" section.

Mohammad Baraheni: Writing- The "machining" section.

Mohammad Fotouhi: Writing- review & editing.

Conflict of Interest

The authors declare no conflict of interest.

References

[1] S. Akbari, F. Taheri-Behrooz, M.M. Shokrieh, *Compos. Sci. Technol.* **2014**, *94*, 8.

[2] S. min Ahn, S.Y. Park, Y.C. Kim, K.S. Lee, J.Y. Kim, *J. Mater. Sci.* **2015**, *50*, 7752.

[3] I. Serrano-Munoz, T. Fritsch, T. Mishurova, A. Trofimov, D. Apel, A. Ulbricht, A. Kromm, R. Hesse, A. Evans, G. Bruno, *J. Mater. Sci.* **2021**, *56*, 5845.

[4] H.W. Carpenter, R.G. Reid, R. Paskaramoorthy, *Int. J. Mech. Mater. Des.* **2015**, *11*, 455.

[5] V. Hauk, *Structural and Residual Stress Analysis by Nondestructive Methods* , Elsevier, Amesterdam **1997**.

[6] G. Sih, E. Sommer, W. Dahl, A. McEvily, **1985**.

[7] M.D. Olson, M.R. Hill, B. Clausen, M. Steinzig, T.M. Holden, *Exp. Mech.* **2015**, *55*, 1093.

[8] R.G. Reid, R. Paskaramoorthy, *Compos. Struct.* **2009**, *88*, 388.

[9] P. Mann, H.Y. Miao, A. Gariépy, M. Lévesque, R.R. Chromik, *J. Mater. Sci.* **2015**, *50*, 2284.

[10] H. Chen, H.Y. Lee, C.S. Ku, A.T. Wu, *J. Mater. Sci.* **2016**, *51*, 3600.

[11] X. Wang, D. Xu, H.Y. Liu, H. Zhou, Y.W. Mai, J. Yang, E. Li, *J. Mater. Sci.* **2016**, *51*, 334.

[12] M. Baraheni, A. Tabatabaeian, S. Amini, A.R. Ghasemi, *Compos. Part B Eng.* **2019**, *172*, 612.

[13] M. Baraheni, A. Tabatabaeian, A.R. Ghasemi, S. Amini, *Modares Mech. Eng.* **2020**, *20*, 1731.

[14] M.X. Yang, R.G. Li, P. Jiang, F.P. Yuan, Y.D. Wang, Y.T. Zhu, X.L. Wu, *Mater. Res. Lett.* **2019**, *7*, 433.

[15] J.A. Francis, J.A. Francis, **2016**, *0836*.

[16] W. Reimers, A.R. Pyzalla, A.K. Schreyer, H. Clemens, *Neutrons Synchrotron Radiat. Eng. Mater. Sci. From Fundam. to Mater. Compon. Charact.* **2008**, 1.

[17] W. Wong, M.R. Hill, **2013**, 339.

[18] G.S. Schajer, *Exp. Mech.* **2010**, *50*, 1117.

[19] G.S. Schajer, *Exp. Mech.* **2010**, *50*, 159.

[20] Z. Zhang, H. Wei, Y. Liu, J. Leng, *Struct. Heal. Monit.* **2015**, *14*, 127.

[21] J. Wissman, A. Perez-rosado, A. Edgerton, B.M. Levi, Z.N. Karakas, M. Kujawski, A. Philipps, N. Papavizas, D. Fallon, H.A. Bruck, E. Smela, *SMART Mater. Struct.* **2013**, *22*.

[22] J.M. Chem, D.R.T. Roberts, S.J. Holder, *J. Mater. Chem* **2011**, 8256.

[23] S. Zeng, D. Zhang, W. Huang, Z. Wang, S.G. Freire, X. Yu, A.T. Smith, E.Y. Huang, H. Nguon, L. Sun, *Nat. Commun.* **2016**, *7*, 1.

[24] D.W. Brown, T.M. Holden, B. Clausen, M.B. Prime, T.A. Sisneros, H. Swenson, J. Vaja, *Acta Mater.* **2011**, *59*, 864.

[25] M. Smith, J.B. Levesque, L. Bichler, D. Sediako, J. Gholipour, P. Wanjara, *Mater. Sci. Eng. A* **2017**, *691*, 168.

[26] N.S. Rossini, M. Dassisti, K.Y. Benyounis, A.G. Olabi, *Mater. Des.* **2012**, *35*, 572.

[27] M.B. Prime, *J. Eng. Mater. Technol. Trans. ASME* **2001**, *123*, 162.

[28] D. Thibault, P. Bocher, M. Thomas, M. Gharghouri, M. Côté, *Mater. Sci. Eng. A* **2010**, *527*, 6205.

[29] M. Pavan, D. Furfari, B. Ahmad, M.A. Gharghouri, M.E. Fitzpatrick, *Int. J. Fatigue* **2019**, *123*, 157.

[30] W. Woo, G.B. An, V.T. Em, A.T. De Wald, M.R. Hill, *J. Mater. Sci.* **2014**, *50*, 784.

[31] M.D. Olson, J.S. Robinson, R.C. Wimpory, M.R. Hill, *Mater. Sci. Technol. (United Kingdom)* **2016**, *32*, 1427.

[32] P. Pagliaro, M.B. Prime, H. Swenson, B. Zuccarello, *Exp. Mech.* **2010**, *50*, 187.

[33] C. Liu, X. Yi, *Mater. Des.* **2013**, *46*, 366.

[34] F. Hosseinzadeh, P. Ledgard, P.J. Bouchard, *Exp. Mech.* **2013**, *53*, 829.

[35] O. Muránsky, C.J. Hamelin, F. Hosseinzadeh, M.B. Prime, *Int. J. Press. Vessel. Pip.* **2017**.

[36] O. Muránsky, F. Hosseinzadeh, C.J. Hamelin, Y. Traore, P. Bendeich, *Int. J. Press. Vessel. Pip.* **2017**.

[37] Y. Wan, W. Jiang, J. Li, G. Sun, D.K. Kim, W. Woo, S.T. Tu, *Mater. Sci. Eng. A* **2017**, *699*, 62.

[38] Y.L. Sun, M.J. Roy, A.N. Vasileiou, M.C. Smith, J.A. Francis, F. Hosseinzadeh, *Exp. Mech.* **2017**, *57*, 719.

[39] M.D. Olson, A.T. DeWald, M.B. Prime, M.R. Hill, *Exp. Mech.* **2015**, *55*, 577.

[40] C.R. D'Elia, S.S. Carlson, M.L. Stanfield, M.B. Prime, J. Araújo de Oliveira, T.J. Spradlin, J.B. Lévesque, M.R. Hill, *Exp. Mech.* **2020**.

[41] H. Wang, D.K. Kim, W. Woo, S.H. Choi, S.Y. Lee, S.K. Hwang, *J. Mech. Sci. Technol.* **2020**, *34*, 1989.

[42] A. Tabatabaeian, A.R. Ghasemi, B. Asghari, *Polym. Test.* **2019**, *80*, 106147.

[43] S. Akbari, F. Taheri-Behrooz, M.M. Shokrieh, *Exp. Mech.* **2013**, *53*, 1509.

[44] Y. Zhang, D. Nelson, *Exp. Mech.* **2017**, *57*, 967.

[45] M.M. Shokrieh, S. Akbari R, *J. Eng. Mater. Technol. Trans. ASME* **2012**, *134*, 1.

[46] M.M. Shokrieh, S. Akbari, *J. Compos. Mater.* **2014**, *48*, 791.

[47] A.H. Mahmoudi, S. Heyarian, K. Behnam, *Mater. Sci. Forum* **2014**, *768–769*, 107.

[48] G.S. Schajer, M.B. Prime, *J. Eng. Mater. Technol.* **2006**, *128*, 375.

[49] C. Can Aydýner, M.B. Prime, *J. Eng. Mater. Technol. Trans. ASME* **2013**, *135*.

[50] A.H. Mahmoudi, M.R. Sheikhpour, S. Heydarian, *Exp. Mech.* **2014**, *54*, 1237.

[51] A.H. Mahmoudi, A.R. Hasani, *J. Strain Anal. Eng. Des.* **2017**, *52*, 93.

[52] M.D. Olson, M.R. Hill, *Exp. Mech.* **2015**, *55*, 1139.

[53] M. Kotobi, M. Honarpisheh, *J. Strain Anal. Eng. Des.* **2017**, *52*, 83.

[54] M.M. Shokrieh, M.A. Kamangar, *J. Eng. Mater. Technol. Trans. ASME* **2016**, *138*, 1.

[55] M.M. Shokrieh, S.M. Jalili, M.A. Kamangar, *Int. J. Mech. Sci.* **2018**, *148*, 383.

[56] S.D. Salehi, M.A. Rastak, M.M. Shokrieh, L. Barrallier, R. Kubler, *Exp. Mech.* **2020**.

[57] M.M. Shokrieh, A. Ghasemi, *J. Compos. Mater.* **2007**.

[58] A. Ghasemi, F. Taheri-Behrooz, M. Shokrieh, *J. Compos. Mater.* **2014**, *48*, 415.

[59] F. Hosseinzadeh, S. Hossain, C.E. Truman, D.J. Smith, *Exp. Mech.* **2014**, *54*, 1151.

[60] A. Magnier, B. Scholtes, T. Niendorf, *Polym. Test.* **2017**, *59*, 29.

[61] T. Wu, S.R. Tinkloh, T. Tröster, W. Zinn, T. Niendorf, *J. Compos. Sci. 2020, Vol. 4, Page 143* **2020**, *4*, 143.

[62] G. Petrucci, M. Scafidi, *Exp. Mech.* **2011**, *51*, 1039.

[63] A.R. Ghasemi, M.M. Mohammadi, *Int. J. Mech. Sci.* **2016**.

[64] A. Magnier, B. Scholtes, T. Niendorf, *Polym. Test.* **2018**, *71*, 329.

[65] A. Magnier, T. Wu, S.R. Tinkloh, T. Tröster, B. Scholtes, T. Niendorf, *Polym. Test.* **2021**, *97*, 107146.

[66] B. Winiarski, P.J. Withers, *Exp. Mech.* **2012**, *52*, 417.

[67] G.S. Schajer, B. Winiarski, P.J. Withers, *Exp. Mech.* **2013**, *53*, 255.

[68] A. Baldi, *Exp. Mech.* **2014**, *54*, 379.

[69] A. Baldi, *Exp. Mech.* **2019**, *59*, 1007.

[70] J.S. Harrington, G.S. Schajer, *Exp. Mech.* **2017**, 559.

[71] S.M. Hosseini, S. Akbari, M.M. Shokrieh, *Microelectron. Reliab.* **2019**, *102*, 113473.

[72] A. Nau, D. von Mirbach, B. Scholtes, *Exp. Mech.* **2013**, *53*, 1371.

[73] S. Schuster, J. Gibmeier, *Exp. Mech.* **2016**, *56*, 369.

[74] G.S. Schajer, C. Abraham, **2014**, 1515.

[75] G.S. Schajer, *Exp. Mech.* **2020**, *60*, 665.

[76] R. Blödorn, M.R. Viotti, R.B. Schroeter, A. Albertazzi, *Exp. Mech.* **2015**, *55*, 1745.

[77] M. Steinzig, D. Upshaw, J. Rasty, *Exp. Mech.* **2014**, *54*, 1537.

[78] G.S. Schajer, **2020**.

[79] T.C. Smit, R.G. Reid, **2018**.

[80] T.C. Smit, R.G. Reid, *Exp. Mech.* **2020**.

[81] T.C. Smit, R.G. Reid, *Exp. Mech.* **2020**.

[82] A. Baldi, *Exp. Mech.* **2016**, *56*, 1191.

[83] K. Masláková, F. Trebuňa, P. Frankovský, M. Binda, *Procedia Eng.* **2012**, *48*, 396.

[84] J.G. Zhu, H.M. Xie, Y.J. Li, Z.X. Hu, Q. Luo, C.Z. Gu, *Exp. Mech.* **2014**, *54*, 127.

[85] M. Sebastiani, A.M. Korsunsky, C. Eberl, E. Bemporad, G.M. Pharr, *Exp. Mech.* **2014**, *54*, 1305.

[86] M. Sebastiani, F. Massimi, G. Merlati, E. Bemporad, *Dent. Mater.* **2015**, *31*, 1396.

[87] F. Archie, M.Z. Mughal, M. Sebastiani, E. Bemporad, S. Zaefferer, *Acta Mater.* **2018**, *150*, 327.

[88] E. Salvati, T. Sui, A.M. Korsunsky, *Int. J. Solids Struct.* **2016**, *87*, 61.

[89] E. Salvati, A.M. Korsunsky, *Int. J. Plast.* **2017**, *98*, 123.

[90] A.J.G. Lunt, N. Baimpas, E. Salvati, I.P. Dolbnya, T. Sui, S. Ying, H. Zhang, A.K. Kleppe, J. Dluhos, A.M. Korsunsky, *J. Strain Anal. Eng. Des.* **2015**.

[91] J. Everaerts, E. Salvati, A.M. Korsunsky, *Adv. Mater. Interfaces* **2019**, *6*, 1900947.

[92] M. Sebastiani, E. Rossi, M.Z. Mughal, A. Benedetto, P. Jacquet, E. Salvati, A.M. Korsunsky,

Nanomater. 2020, Vol. 10, Page 853 **2020**, *10*, 853.

[93] R. Ali, M. Renzelli, M.I. Khan, M. Sebastiani, E. Bemporad, *Nanomater. 2018, Vol. 8, Page 896* **2018**, *8*, 896.

[94] F. Menda, P. Šarga, T. Lipták, F. Trebuna, *Procedia Eng.* **2014**, *96*, 289.

[95] B. Zuccarello, F. Menda, M. Scafidi, *Exp. Mech.* **2016**, *56*, 1531.

[96] R. Moharrami, M. Sadri, *Strain* **2018**, *54*, 1.

[97] C. Bouffioux, R. Pesci, R. Boman, N. Caillet, J.P. Ponthot, A.M. Habraken, *Thin-Walled Struct.* **2016**, *104*, 126.

[98] A. Giri, M.M. Mahapatra, *Measurement* **2017**, *106*, 152.

[99] M. Barsanti, M. Beghini, C. Santus, A. Benincasa, L. Bertelli, *J. Strain Anal. Eng. Des.* **2018**, *53*, 210.

[100] M.W. Hyer, *J. Compos. Mater.* **1981**, *15*, 175.

[101] M.W. Hyer, *J. Compos. Mater.* **1982**, *16*, 318.

[102] M. Mobarakian, M. Safarabadi, M. Farahani, *Compos. Struct.* **2020**, *236*, 111875.

[103] M.M. Shokrieh, A. Daneshvar, S. Akbari, M. Chitsazzadeh, *Carbon N. Y.* **2013**, *59*, 255.

[104] A.R. Ghasemi, M.M. Fesharaki, *Iran. Polym. J.* **2018**, *0*, 0.

[105] A.R. Ghasemi, M. Mohammadi-Fesharaki, *Polym. Bull.* **2019**.

[106] A. Tabatabaeian, A.R. Ghasemi, *Mech. Mater.* **2019**, *131*, 69.

[107] A. Tabatabaeian, A.R. Ghasemi, *Polym. Bull.* **2020**.

[108] A. Tabatabaeian, M. Lotfi, A.R. Ghasemi, S. Rooholahi, *Eng. Struct.* **2020**, *228*, 111490.

[109] C. Genzel, I.A. Denks, M. Klaus, *Mod. Diffr. Methods* **2012**, 127.

[110] C.J. Bechtoldt, R.C. Placious, W.J. Boettinger, M. Kuriyama, *Adv. X-Ray Anal.* **1981**, *25*, 329.

[111] A. Liehr, W. Zinn, S. Degener, B. Scholtes, T. Niendorf, C. Genzel, *HTM J. Heat Treat. Mater.* **2017**, *72*, 115.

[112] S. Tadano, B. Giri, *Sci. Technol. Adv. Mater.* **2011**, *12*, 064708.

[113] J.S. Robinson, W. Redington, *Mater. Charact.* **2015**, *105*, 47.

[114] V.A.N. Righetti, T.M.B. Campos, L.B. Robatto, R.R. Rego, G.P. Thim, *Exp. Mech.* **2020**, *60*, 475.

[115] H. Hizli, C.H. GÜR, *Res. Nondestruct. Eval.* **2018**, *29*, 221.

[116] E. Salvati, A.J.G. Lunt, S. Ying, T. Sui, H.J. Zhang, C. Heason, G. Baxter, A.M. Korsunsky, *Comput. Methods Appl. Mech. Eng.* **2017**, *320*, 335.

[117] E. Salvati, T. Sui, H. Zhang, A.J.G. Lunt, K.S. Fong, X. Song, A.M. Korsunsky, *Adv. Eng. Mater.* **2016**, *18*, 2076.

[118] E. Salvati, J. Everaerts, K. Kageyama, A.M. Korsunsky, *Fatigue Fract. Eng. Mater. Struct.* **2019**, *42*, 1980.

[119] E. Salvati, H. Zhang, K.S. Fong, X. Song, A.M. Korsunsky, *J. Mech. Phys. Solids* **2017**, *98*, 222.

[120] M. Meindlhumer, N. Jäger, S. Spor, M. Rosenthal, J.F. Keckes, H. Hruby, C. Mitterer, R. Daniel, J. Keckes, J. Todt, *Scr. Mater.* **2020**, *182*, 11.

[121] M. Meindlhumer, L.R. Brandt, J. Zalesak, M. Rosenthal, H. Hruby, J. Kopecek, E. Salvati, C. Mitterer, R. Daniel, J. Todt, J. Keckes, A.M. Korsunsky, *Mater. Des.* **2021**, *198*, 109365.

[122] A. Steuwer, J.R. Santisteban, M. Turski, P.J. Withers, T. Buslaps, *J. Appl. Cryst* **2004**, *37*, 883.

[123] I.C.. Noyan, J.B. Cohen, *Residual Stress: Measurement by Diffraction and Interpretation* , Springer-Verlag**1987**.

[124] A. Steuwer, J.R. Santisteban, M. Turski, P.J. Withers, T. Buslaps, *Nucl. Instruments Methods Phys. Res. Sect. B Beam Interact. with Mater. Atoms* **2005**, *238*, 200.

[125] P. Ji, J. Zhang, L. Zheng, Y. Xiao, S. Dou, X. Cui, Y. Lian, *J. Mater. Sci.* **2017**, *52*, 12834.

[126] T. Manns, B. Scholtes, *Thin Solid Films* **2013**, *530*, 53.

[127] W. Song, C. Xu, Q. Pan, J. Song, *Chinese J. Mech. Eng. 2016 292* **2015**, *29*, 365.

[128] Y. Javadi, M. Akhlaghi, M.A. Najafabadi, *Mater. Des.* **2013**, *45*, 628.

[129] Y. Zhan, C. Liu, X. Kong, Z. Lin, *Ultrasonics* **2017**, *73*, 271.

[130] C. Xu, W. Song, Q. Pan, H. Li, S. Liu, *Phys. Procedia* **2015**, *70*, 594.

[131] H.L. Ma, K. tak Lau, D. Hui, S. qiang Shi, C. kin Poon, *Compos. Part B Eng.* **2017**, *128*, 67.

[132] M.M. Shokrieh, S. Akbari, A. Daneshvar, *Compos. Struct.* **2013**, *96*, 708.

[133] R. Ghaedamini, A. Ghassemi, A. Atrian, *Arch. Appl. Mech.* **2018**, *88*, 755.

[134] K. Zhang, Z. Yang, Y. Li, C. Al, *Int. J. Adhes. Adhes.* **2013**, *46*, 7.

[135] A.R. Ghasemi, A. Tabatabaeian, M. Moradi, *J. Compos. Mater.* **2018**.

[136] G.C. Papanicolaou, M. V Michalopoulou, N.K. Anifantis, **2002**, *62*, 1881.

[137] M.M. Shokrieh, M. Safarabadi, *J. Strain Anal. Eng. Des.* **2011**, *46*, 817.

[138] M. Epstein, **2002**, *29*, 501.

[139] M.Y. Quek, **2004**, *24*, 379.

[140] I. Baran, J.H. Hattel, R. Akkerman, *Compos. Part B* **2015**, *68*, 365.

[141] A. Ding, S. Li, J. Wang, L. Zu, *Compos. Struct.* **2015**, *129*, 60.

[142] H. Ledbetter, M.L. Dunn, **2000**, *285*, 180.

[143] I. Baran, R. Akkerman, J.H. Hattel, *Compos. Struct.* **2014**, *118*, 37.

[144] J. Merodio, R.W. Ogden, J. Rodríguez, *Int. J. Non. Linear. Mech.* **2013**, *56*, 43.

[145] M. Liu, H. Ruan, L. Zhang, A. Moridi, *J. Mater. Res.* **2012**, *27*, 2737.

[146] A. Moridi, H. Ruan, L.C. Zhang, M. Liu, *Int. J. Solids Struct.* **2013**, *50*, 3562.

[147] M. Sedighi, J. Joudaki, H. Kheder, *J. Strain Anal. Eng. Des.* **2017**, *52*, 102.

[148] Y. Song, W. Wu, F. Xie, Y. Liu, T. Wang, *PLoS One* **2017**, *12*, 1.

[149] A. Jafarpour, M. Safarabadi, M. Haghighi-Yazdi, A. Yousefi, *Mech. Adv. Mater. Struct.* **2020**, *0*, 1.

[150] M. Safarabadi, *J. Compos. Mater.* **2016**, *50*, 3753.

[151] V. Teimouri, M. Safarabadi, *Eng. Solid Mech.* **2018**, *6*, 11.

[152] S. Brunbauer, G. Winter, T. Antretter, P. Staron, W. Ecker, *Mater. Sci. Eng. A* **2019**, *747*, 73.

[153] M. Mobarakian, M. Safarabadi, M. Farahani, *Polym. Test.* **2020**, *87*, 106503.

[154] A. Tabatabaeian, M. Baraheni, S. Amini, A.R. Ghasemi, *J. Compos. Mater.* **2019**, 002199831984481.

[155] A.R. Ghasemi, A. Tabatabaeian, M. Moradi, *J. Compos. Mater.* **2020**.

[156] X. Jiang, W. Xiong, L. Wang, M. Guo, Z. Ding, *Mater. Sci. Technol. (United Kingdom)* **2020**, *36*, 168.

[157] J.H. Moon, S.M. Baek, S.G. Lee, Y. Seong, A. Amanov, S. Lee, H.S. Kim, *Mater. Res. Lett.* **2019**, *7*, 97.

[158] Y. Liu, W. Wang, Y.F. Chen, H. Ji, *Constr. Build. Mater.* **2016**, *129*, 37.

[159] Y. Yi, Q. Li, J. Xing, H. Fu, D. Yi, Y. Liu, B. Zheng, *Mater. Sci. Eng. A* **2019**, *754*, 129.

[160] J.S. Robinson, T. Pirling, C.E. Truman, T. Panzner, *Mater. Sci. Technol. (United Kingdom)* **2017**, *33*, 1765.

[161] J.S. Robinson, R.C. Wimpory, *Mater. Sci. Technol. (United Kingdom)* **2019**, *35*, 1381.

[162] B. Asghari, A.R. Ghasemi, A. Tabatabaeian, *Compos. Sci. Technol.* **2019**, 107743.

[163] S. Amir-Ahmadi, A.R. Ghasemi, *J. Compos. Mater.* **2020**.

[164] M. Péron, F. Jacquemin, P. Casari, G. Orange, J. Bikard, J.L. Bailleul, N. Boyard, *Compos. Part A Appl. Sci. Manuf.* **2020**, *137*, 106039.

[165] J.S. Robinson, C.E. Truman, A. O'Donovan, J. Rebelo Kornmeier, *Mater. Sci. Technol. (United Kingdom)* **2019**, *35*, 1864.

[166] A.R. Ghasemi, A. Tabatabaeian, B. Asghari, *Mech. Mater.* **2019**, *134*, 185.

[167] A. Kotousov, *Int. J. Fract.* **2000**, *103*, 361.

[168] M.C. Smith, O. Muránsky, Q. Xiong, P.J. Bouchard, J. Mathew, C. Austin, *Int. J. Press. Vessel. Pip.* **2019**, *172*, 233.

[169] W. Woo, G.B. An, E.J. Kingston, A.T. Dewald, D.J. Smith, M.R. Hill, *Acta Mater.* **2013**, *61*, 3564.

[170] Y. Javadi, J.N. Walsh, A. Elrefaey, M.J. Roy, J.A. Francis, *Int. J. Press. Vessel. Pip.* **2017**, *154*, 58.

[171] G. Yan, A. Crivoi, Y. Sun, N. Maharjan, X. Song, F. Li, M.J. Tan, *J. Manuf. Process.* **2018**, *32*, 763.

[172] S. Paddea, J.A. Francis, A.M. Paradowska, P.J. Bouchard, I.A. Shibli, *Mater. Sci. Eng. A* **2012**,

534, 663.

[173] F. Uzun, A.M. Korsunsky, *Mater. Sci. Eng. A* **2019**, *752*, 180.

[174] B. Chen, A. Skouras, Y.Q. Wang, J.F. Kelleher, S.Y. Zhang, D.J. Smith, P.E.J. Flewitt, M.J. Pavier, *Mater. Sci. Eng. A* **2014**, *590*, 374.

[175] C. Pandey, M.M. Mahapatra, P. Kumar, *Arch. Civ. Mech. Eng.* **2018**, *18*, 1000.

[176] T. Ramjaun, H.J. Stone, L. Karlsson, J. Kelleher, R.J. Moat, J.R. Kornmeier, K. Dalaei, H.K.D.H. Bhadeshia, *Sci. Technol. Weld. Join.* **2014**, *19*, 44.

[177] L. Gannon, Y. Liu, N. Pegg, M. Smith, *Mar. Struct.* **2010**, *23*, 385.

[178] H. Alipooramirabad, R. Ghomashchi, A. Paradowska, M. Reid, *J. Mater. Process. Technol.* **2016**, *231*, 456.

[179] G. Fu, M.I. Lourenço, M. Duan, S.F. Estefen, *Mar. Struct.* **2016**, *46*, 30.

[180] H. Alipooramirabad, A. Paradowska, R. Ghomashchi, M. Reid, *J. Manuf. Process.* **2017**, *28*, 70.

[181] W.C. Jiang, B.Y. Wang, J.M. Gong, S.T. Tu, *Mater. Des.* **2011**, *32*, 2851.

[182] H. Alipooramirabad, A. Paradowska, R. Ghomashchi, A. Kotousov, M. Reid, *J. Mater. Process. Technol.* **2015**, *226*, 40.

[183] M.D. Olson, M.R. Hill, E. Willis, A.G. Peterson, V.I. Patel, O. Muránsky, *J. Nucl. Eng. Radiat. Sci.* **2015**, *1*, 1.

[184] M.R. Hill, M.D. Olson, A.T. DeWald, *J. Press. Vessel Technol. Trans. ASME* **2016**, *138*, 1.

[185] W. Woo, G.B. An, C.E. Truman, W. Jiang, M.R. Hill, *J. Mater. Sci.* **2016**, *51*, 10620.

[186] M. Moattari, M.M. Shokrieh, H. Moshayedi, H. Kazempour-Liasi, *J. Therm. Stress.* **2020**, *43*, 801.

[187] M. Moattari, M.M. Shokrieh, H. Moshayedi, *Theor. Appl. Fract. Mech.* **2020**, *108*, 102614.

[188] G. Salerno, C. Bennett, W. Sun, A. Becker, N. Palumbo, J. Kelleher, S.Y. Zhang, *Int. J. Mech. Sci.* **2018**, *144*, 654.

[189] M.C. Smith, P.J. Bouchard, M. Turski, L. Edwards, R.J. Dennis, *Comput. Mater. Sci.* **2012**, *54*, 312.

[190] D. Yan, A. Wu, J. Silvanus, Q. Shi, *Mater. Des.* **2011**, *32*, 2284.

[191] K. Ogawa, D. Deng, S. Kiyoshima, N. Yanagida, K. Saito, *Comput. Mater. Sci.* **2009**, *45*, 1031.

[192] D. Deng, H. Murakawa, M. Shibahara, *Comput. Mater. Sci.* **2010**, *48*, 187.

[193] D. Deng, *Mater. Des.* **2013**, *49*, 1022.

[194] J. Mathew, R.J. Moat, S. Paddea, J.A. Francis, M.E. Fitzpatrick, P.J. Bouchard, *Metall. Mater. Trans. A Phys. Metall. Mater. Sci.* **2017**, *48*, 6178.

[195] J. Mathew, R.J. Moat, S. Paddea, M.E. Fitzpatrick, P.J. Bouchard, *Int. J. Press. Vessel. Pip.* **2017**, *150*, 89.

[196] V. Akrivos, R.C. Wimpory, M. Hofmann, B. Stewart, O. Muransky, M.C. Smith, J. Bouchard, *J. Appl. Crystallogr.* **2020**, *53*, 1.

[197] J.R. Chukkan, G. Wu, M.E. Fitzpatrick, S. Jones, J. Kelleher, *Int. J. Mech. Sci.* **2019**, *160*, 421.

[198] E. Almeida, *Ind. Eng. Chem. Res.* **2001**, *40*, 3.

[199] F. Fanicchia, X. Maeder, J. Ast, A.A. Taylor, Y. Guo, M.N. Polyakov, J. Michler, D.A. Axinte, *Mater. Des.* **2018**, *153*, 36.

[200] W. Luo, U. Selvadurai, W. Tillmann, *J. Therm. Spray Technol.* **2016**, *25*, 321.

[201] A.A. Abubakar, A.F.M. Arif, K.S. Al-Athel, S.S. Akhtar, J. Mostaghimi, *J. Therm. Spray Technol.* **2017**, *26*, 1115.

[202] B. Marzbanrad, E. Toyserkani, H. Jahed, *J. Mater. Process. Technol.* **2021**, 116928.

[203] R. Tucker, in *Handb. Surf. Eng.*, **1993**, 1446.

[204] J.M.M. Herrera Ramirez, R.P.P. Bustamante, C.A.A. Isaza Merino, A.M.. Arizmendi Morquecho, *Cham, Switz.* **2020**.

[205] M. Halmi, M. Harimon, L. Mohd Tobi, M. Mahmod, *Int. J. Mech. Eng. Technol.* **2019**, *10*, 1285.

[206] O. Kovářík, P. Haušild, J. Siegl, J. Matějíček, V. Davydov, *Procedia Mater. Sci.* **2014**, *3*, 586.

[207] H.C. Back, J. Gibmeier, R. Vaßen, *J. Therm. Spray Technol.* **2020**, *29*, 1242.

[208] M. Floristán, R. Fontarnau, A. Killinger, R. Gadow, *Surf. Coatings Technol.* **2010**, *205*, 1021.

[209] V. Lasseur, S. Goutier, V. Martinez Garcia, A. Denoirjean, E. Meillot, G. Mariaux, J. Absi, A. Killinger, *J. Therm. Spray Technol.* **2020**, *29*, 1313.

[210] J.G. Thakare, R.S. Mulik, M.M. Mahapatra, *Arch. Civ. Mech. Eng.* **2020**, *20*.

[211] M. Pang, X.H. Zhang, Q.X. Liu, Y.X. Fu, G. Liu, W.D. Tan, *Surf. Coatings Technol.* **2020**, *385*, 125377.

[212] M.S. Zoei, T. Farizeh, M.H. Sadeghi, M. Salehi, *J. Therm. Spray Technol.* **2020**, *29*, 1351.

[213] T.A. Owoseni, M. Bai, N. Curry, E.H. Lester, D.M. Grant, T. Hussain, *J. Therm. Spray Technol.* **2020**, *29*, 1339.

[214] M. Jalali Azizpour, M. Tolouei-Rad, *Mater. Res. Express* **2019**, *6*.

[215] M. Gui, R. Eybel, S. Radhakrishnan, F. Monerie-Moulin, R. Raininger, P. Taylor, *J. Therm. Spray Technol.* **2019**, *28*, 1295.

[216] V. Luzin, K. Spencer, M.X. Zhang, *Acta Mater.* **2011**, *59*, 1259.

[217] A. Papyrin, V. Kosarev, S. Klinkov, A. Alkhimov, V.M. Fomin, *Cold Spray Technology*, **2007**.

[218] A.W.Y. Tan, W. Sun, A. Bhowmik, J.Y. Lek, X. Song, W. Zhai, H. Zheng, F. Li, I. Marinescu, Z. Dong, E. Liu, *J. Therm. Spray Technol.* **2019**, *28*, 1959.

[219] B. Marzbanrad, H. Jahed, E. Toyserkani, *Mater. Des.* **2018**, *138*, 90.

[220] A. Bhowmik, A. Wei-Yee Tan, W. Sun, Z. Wei, I. Marinescu, E. Liu, *Results Mater.* **2020**, *7*, 100119.

[221] A. Moridi, S.M. Hassani-Gangaraj, S. Vezzú, L. Trško, M. Guagliano, *Surf. Coatings Technol.* **2015**, *283*, 247.

[222] F. Khodabakhshi, B. Marzbanrad, L.H. Shah, H. Jahed, A.P. Gerlich, *J. Therm. Spray Technol.* **2019**, *28*, 1185.

[223] F. Khodabakhshi, B. Marzbanrad, A. Yazdanmehr, H. Jahed, A.P. Gerlich, *Surf. Coatings Technol.* **2019**, *380*, 125008.

[224] A. Vargas-Uscategui, P.C. King, M.J. Styles, M. Saleh, V. Luzin, K. Thorogood, *J. Therm. Spray Technol.* **2020**, *29*, 1508.

[225] B. Marzbanrad, M.H. Razmpoosh, E. Toyserkani, H. Jahed, *J. Magnes. Alloy.* **2021**.

[226] B. Marzbanrad, E. Toyserkani, H. Jahed, *Key Eng. Mater.* **2019**, *813 KEM*, 411.

[227] B. Marzbanrad, E. Toyserkani, H. Jahed, *Surf. Coatings Technol.* **2021**, *416*, 127155.

[228] J. Bowden, D; Halley, **2001**.

[229] Z. Zhang, L. Li, Y. Yang, N. He, W. Zhao, *Int. J. Adv. Manuf. Technol.* **2014**, *73*, 1765.

[230] S. Masoudi, S. Amini, E. Saeidi, H. Eslami-Chalander, *Int. J. Adv. Manuf. Technol.* **2014**, *76*, 597.

[231] M.B. Prime, M.R. Hill, *Scr. Mater.* **2002**, *46*, 77.

[232] E. Salvati, A.M. Korsunsky, *J. Mater. Process. Technol.* **2020**, *275*, 116373.

[233] S. Chupakhin, N. Kashaev, N. Huber, *J. Strain Anal. Eng. Des.* **2016**, 1.

[234] R.B. Azhiri, A.S. Bideskan, F. Javidpour, R.M. Tekiyeh, *Int. J. Adv. Manuf. Technol.* **2019**, *101*, 2849.

[235] A.L. Mantle, D.K. Aspinwall, *J. Mater. Process. Technol.* **2001**, *118*, 143.

[236] P. Dahlman, *J. Mater. Process. Technol.* **2004**, *147*, 181.

[237] R.M. Arunachalam, M.A. Mannan, A.C. Spowage, *Int. J. Mach. Tools Manuf.* **2004**, *44*, 879.

[238] M. Liu, J.I. Takagi, A. Tsukuda, *J. Mater. Process. Technol.* **2004**, *150*, 234.

[239] T. Özel, E. Zeren, *Int. J. Adv. Manuf. Technol.* **2007**, *35*, 255.

[240] H. Guo, D.W. Zuo, H.B. Wu, F. Xu, G.Q. Tong, *Mater. Sci. Eng. A* **2009**, *499*, 230.

[241] Z.T. Tang, Z.Q. Liu, Y.Z. Pan, Y. Wan, X. Ai, *J. Mater. Process. Technol.* **2009**, *209*, 4502.

[242] J. guang Li, S. qi Wang, *Int. J. Adv. Manuf. Technol.* **2017**, *89*, 997.

[243] J.E. Wyatt, J.T. Berry, *J. Mater. Process. Technol.* **2006**, *171*, 132.

[244] B. Rao, Y.C. Shin, *Int. J. Mach. Tools Manuf.* **2001**, *41*, 1763.

[245] M. Nasr, E.G. Ng, M. Elbestawi, *Proc. Inst. Mech. Eng. Part B J. Eng. Manuf.* **2007**, *221*, 1387.

[246] M.H. Hajmohammad, A. Tabatabaeian, A.R. Ghasemi, F. Taheri-Behrooz, *Compos. Part B* **2020**, *183*, 107732.

[247] A.R. Ghasemi, A. Tabatabaeian, M.H. Hajmohammad, F. Tornabene, *Compos. Struct.* **2021**, *273*, 114280.

[248] A. Pramanik, L.C. Zhang, J.A. Arsecularatne, *Int. J. Mach. Tools Manuf.* **2008**, *48*, 1613.

[249] K. Lin, W. Wang, R. Jiang, Y. Xiong, *Int. J. Adv. Manuf. Technol.* **2019**, *100*, 143.

[250] E. Capello, *J. Mater. Process. Technol.* **2005**, *160*, 221.

[251] E. Capello, *J. Mater. Process. Technol.* **2006**, *172*, 319.

[252] V. Sharma, P.M. Pandey, *Ultrasonics* **2016**, *70*, 172.

[253] D. Zhang, JY; Liang, SY; Zhang, G; Yen, *Mater. Manuf. Process.* **2006**, *21*, 39.

[254] F. Jafarian, H. Amirabadi, J. Sadri, H.R. Banooie, *Mater. Manuf. Process.* **2014**, *29*, 337.

[255] M. Wan, X.Y. Ye, D.Y. Wen, W.H. Zhang, *J. Mater. Sci.* **2019**, *54*.

[256] R. Teimouri, Z. Liu, *Int. J. Adv. Manuf. Technol.* **2020**.

[257] Z. Pan, Y. Feng, X. Ji, S.Y. Liang, *Mach. Sci. Technol.* **2018**, *22*, 507.

[258] Y. Ma, P. Feng, J. Zhang, Z. Wu, D. Yu, *J. Mater. Process. Technol.* **2016**, *235*, 41.

[259] Z. Liu, M. Yang, J. Deng, M. Zhang, Q. Dai, *Int. J. Adv. Manuf. Technol.* **2020**, *106*, 4203.

[260] R. Teimouri, S. Amini, M. Guagliano, *Mater. Sci. Eng. A* **2019**, *747*, 208.

[261] Y. Wei, X.W. Wang, *Int. J. Adv. Manuf. Technol.* **2007**, *33*, 260.

[262] F. Jafarian, *J. Brazilian Soc. Mech. Sci. Eng.* **2019**, *41*, 1.

[263] Z. Pan, S.Y. Liang, H. Garmestani, *Proc. Inst. Mech. Eng. Part B J. Eng. Manuf.* **2019**, *233*, 1103.

[264] Z. Xiao, C. Chen, H. Zhu, Z. Hu, B. Nagarajan, L. Guo, X. Zeng, *Mater. Des.* **2020**, *193*, 108846.

[265] Y. Li, K. Zhou, P. Tan, S.B. Tor, C.K. Chua, K.F. Leong, *Int. J. Mech. Sci.* **2018**, *136*, 24.

[266] Q. Wu, T. Mukherjee, A. De, T. DebRoy, *Addit. Manuf.* **2020**, *35*, 101355.

[267] C. Zhang, C. Shen, X. Hua, F. Li, Y. Zhang, Y. Zhu, *Int. J. Adv. Manuf. Technol. 2020 1113* **2020**, *111*, 797.

[268] S. Srivastava, R.K. Garg, V.S. Sharma, A. Sachdeva, *Arch. Comput. Methods Eng. 2020 285* **2020**, *28*, 3491.

[269] B. Aminforoughi, S. Degener, J. Richter, A. Liehr, T. Niendorf, *Adv. Eng. Mater.* **2021**, 2100184.

[270] T. Mishurova, K. Artzt, J. Haubrich, S. Evsevleev, A. Evans, M. Meixner, I.S. Munoz, I. Sevostianov, G. Requena, G. Bruno, *Metall. Mater. Trans. A 2020 516* **2020**, *51*, 3194.

[271] J. Schröder, T. Mishurova, T. Fritsch, I. Serrano-Munoz, A. Evans, M. Sprengel, M. Klaus, C. Genzel, J. Schneider, G. Bruno, *Mater. Sci. Eng. A* **2021**, *805*, 140555.

[272] K. Carpenter, A. Tabei, *Materials (Basel).* **2020**, *13*.

[273] M.B. Prime, **2018**, *7*, 19.

[274] F. Hosseinzadeh, J. Kowal, P.J. Bouchard, *J. Eng.* **2014**, *2014*, 453.

[275] M.B. Prime, A.T. DeWald, M.R. Hill, B. Clausen, M. Tran, *Eng. Fract. Mech.* **2014**, *116*, 158.

[276] R.L. Ribeiro, M.R. Hill, *Eng. Fract. Mech.* **2016**, *163*, 313.

[277] F. Appel, J.D.H. Paul, P. Staron, M. Oehring, O. Kolednik, J. Predan, F.D. Fischer, *Mater. Sci. Eng. A* **2018**, *709*, 17.

[278] E. Salvati, *Theor. Appl. Fract. Mech.* **2021**, *114*, 103021.

[279] M.O.C. Villas-Boas, F.C. Serbena, V.O. Soares, I. Mathias, E.D. Zanotto, *J. Am. Ceram. Soc.* **2020**, *103*, 465.

[280] J.C. Kim, S.K. Cheong, H. Noguchi, *Int. J. Fatigue* **2013**, *56*, 114.

[281] J. Zhang, X. Wang, S. Paddea, X. Zhang, *Mater. Des.* **2016**, *90*, 551.

[282] N. Ao, D. Liu, X. Zhang, C. Liu, *Appl. Surf. Sci.* **2019**, *489*, 595.

[283] A.K. Syed, B. Ahmad, H. Guo, T. Machry, D. Eatock, J. Meyer, M.E. Fitzpatrick, X. Zhang, *Mater. Sci. Eng. A* **2019**, *755*, 246.

[284] P. M, A.K. Prasad, M.K. Paswan, *Appl. Mater. Today* **2020**, *19*, 100584.

[285] H. Xin, M. Veljkovic, *Mater. Des.* **2020**, *193*, 108732.

[286] A. Jacob, A. Mehmanparast, R.D. Urzo, J. Kelleher, *Int. J. Fatigue* **2019**, *128*, 105196.

[287] J.A. Ronevich, E. Ju, Z. Feng, Y. Wang, C.D. Elia, M.R. Hill, *Eng. Fract. Mech.* **2020**, *228*, 106846.

[288] R. Goswami, S.B. Qadri, C.R. Feng, C.S. Pande, *Mater. Sci. Eng. A* **2019**, *763*, 138113.

[289] W. Wang, H. Liu, C. Zhu, X. Du, J. Tang, *Int. J. Mech. Sci.* **2019**, *151*, 263.

[290] C. Gu, J. Lian, Y. Bao, S. Münstermann, *Mater. Sci. Eng. A* **2019**, *751*, 133.

[291] M.C.E.P.M.A. Martínez, *Biomech Model Mechanobiol* **2012**, *11*, 1001.

[292] C. Colpitts, A.M. Ektesabi, R.A. Wyatt, B.D. Crawford, A. Kiani, *J. Mech. Behav. Biomed. Mater.* **2017**, *74*, 214.

[293] S. Yamada, S. Tadano, *J. Biomech.* **2013**, *46*, 2130.

[294] B. Conroy, Y. Traoré, S. Paddea, J. Kelleher, D. Tanner, B. Conroy, Y. Traoré, S. Paddea, J. Kelleher, D. Tanner, D. Tanner, **2017**, *0836*.

[295] P.K.M. Tung, S. Mudie, J.E. Daniels, *Acta Biomater.* **2013**, *9*, 9503.

[296] K. Ohmori, T. Tasaki, S. Kimura, A. Hori, N. Sakaeda, M. Hanabusa, T. Yamamoto, *J. Mech. Behav. Biomed. Mater.* **2020**, *104*, 103643.

[297] R.K. Chintapalli, A. Mestra Rodriguez, F. Garcia Marro, M. Anglada, *J. Mech. Behav. Biomed. Mater.* **2014**, *29*, 126.

[298] Y. Zhang, M. Allahkarami, J.C. Hanan, *J. Mech. Behav. Biomed. Mater.* **2012**, *6*, 120.

[299] A.K. Mainjot, G.S. Schajer, A.J. Vanheusden, M.J. Sadoun, *Dent. Mater.* **2012**, *28*, 378.

[300] A.K. Mainjot, A. Najjar, B.D. Jakubowicz-Kohen, M.J. Sadoun, *Dent. Mater.* **2015**, *31*, 1142.

[301] B. Henriques, G. Miranda, M. Gasik, J.C.M. Souza, R.M. Nascimento, F.S. Silva, *J. Mech. Behav. Biomed. Mater.* **2015**, *50*, 123.

[302] M. Wendler, R. Belli, A. Petschelt, U. Lohbauer, *J. Mech. Behav. Biomed. Mater.* **2016**, *60*, 535.

[303] V.P. Fardin, E.A. Bonfante, P.G. Coelho, M.N. Janal, N. Tovar, L. Witek, D. Bordin, G. Bonfante, *Dent. Mater.* **2018**, *34*, 260.

[304] J. Kim, S. Dhital, P. Zhivago, M.R. Kaizer, Y. Zhang, *J. Mech. Behav. Biomed. Mater.* **2018**, *82*, 202.

[305] S. Dhital, C. Rodrigues, Y. Zhang, J. Kim, *J. Mech. Behav. Biomed. Mater.* **2020**, *103*, 103545.

[306] A. Lunt, E. Salvati, N. Baimpas, I. Dolbnya, T.K. Neo, A.M. Korsunsky, *Dent. Mater.* **2019**, *35*, 1576.

[307] M. Inokoshi, F. Zhang, K. Vanmeensel, J. De Munck, S. Minakuchi, I. Naert, J. Vleugels, B. Van Meerbeek, *Dent. Mater.* **2017**, *33*, e147.

[308] S.S. Kim, H. Murayama, K. Kageyama, K. Uzawa, M. Kanai, *Compos. Part A Appl. Sci. Manuf.* **2012**, *43*, 1197.

[309] R. Fernández, S. Cabeza, T. Mishurova, P. Fernández-Castrillo, G. González-Doncel, G. Bruno, *Mater. Sci. Eng. A* **2018**, *731*, 344.

[310] M.M. Shokrieh, A. Daneshvar, S. Akbari, *Mater. Des.* **2014**, *53*, 209.

[311] A.R. Ghasemi, M.M. Mohammadi, M. Mohandes, *Compos. Part B Eng.* **2015**, *77*, 519.

[312] A.R. Ghasemi, B. Asghari, A. Tabatabaeian, *Int. J. Press. Vessel. Pip.* **2020**, *183*, 104098.

[313] A. Jafarpour, M. Safarabadi Farahani, M. Haghighi-Yazdi, *Mech. Mater.* **2019**, *138*, 103176.

[314] D.G. Richards, P.B. Prangnell, P.J. Withers, S.W. Williams, T. Nagy, S. Morgan, *Sci. Technol. Weld. Join.* **2010**, *15*, 156.

[315] J. Lin, N. Ma, X. Liu, Y. Lei, *J. Mater. Process. Technol.* **2020**, *278*, 116504.

[316] S.W. Ooi, J.E. Garnham, T.I. Ramjaun, *Mater. Des.* **2014**, *56*, 773.

[317] R.J. Moat, S. Ooi, A.A. Shirzadi, H. Dai, A.F. Mark, H.K.D.H. Bhadeshia, P.J. Withers, *Mater. Sci. Technol. (United Kingdom)* **2018**, *34*, 519.

[318] X. Song, F. Wang, D. Qian, L. Hua, *Mater. Sci. Eng. A* **2020**, *780*, 139171.

[319] M. Kattoura, A. Telang, S.R. Mannava, D. Qian, V.K. Vasudevan, *Mater. Sci. Eng. A* **2018**, *711*, 364.

[320] S. Breumier, A. Villani, C. Maurice, M. Lévesque, G. Kermouche, *Mater. Des.* **2019**, *169*, 107659.

[321] J. Wu, H. Liu, P. Wei, Q. Lin, S. Zhou, *Int. J. Mech. Sci.* **2020**, *183*.

[322] S.M. Shah, D. Nélias, M. Zain-Ul-Abdein, M. Coret, *Finite Elem. Anal. Des.* **2012**, *61*, 1.

[323] Z. Ding, G. Sun, M. Guo, X. Jiang, B. Li, S.Y. Liang, *J. Mater. Process. Technol.* **2020**, *281*, 116647.

[324] X. Yang, J. Zhu, Z. Nong, Z. Lai, D. He, *Comput. Mater. Sci.* **2013**, *69*, 396.

[325] N. Ahmed, J.W. Murray, T. Yuzawa, T. Kurokawa, T. Nakagawa, S. Sarugaku, D. Saito, A.T. Clare, *Surf. Coatings Technol.* **2021**, *416*, 127156.

[326] J.S. Wang, C.C. Hsieh, H.H. Lai, C.W. Kuo, P.T.Y. Wu, W. Wu, *Mater. Charact.* **2015**, *99*, 248.

[327] J.S. Robinson, M.S. Hossain, C.E. Truman, *J. Strain Anal. Eng. Des.* **2021**.

[328] H. Gao, Y. Zhang, Q. Wu, J. Song, K. Wen, *Int. J. Fatigue* **2018**, *108*, 62.

[329] H. Gao, S. Wu, Q. Wu, B. Li, Z. Gao, Y. Zhang, S. Mo, *Mater. Des.* **2020**, *195*, 108954.

[330] G. Vastola, G. Zhang, Q.X. Pei, Y. Zhang, *Adv. Eng. Mater.* **2017**, *1700333*, 1.

[331] D. Buchbinder, W. Meiners, N. Pirch, K. Wissenbach, J. Schrage, D. Buchbinder, W. Meiners, N. Pirch, K. Wissenbach, *J. Laser Appl.* **2015**, *012004*.

[332] G. Vastola, G. Zhang, Q.X. Pei, Y.W. Zhang, *Addit. Manuf.* **2016**, *12*, 231.

[333] H. Ali, L. Ma, H. Ghadbeigi, K. Mumtaz, *Mater. Sci. Eng. A* **2017**, *695*, 211.

[334] J.D. Roehling, W.L. Smith, T.T. Roehling, B. Vrancken, G.M. Guss, J.T. McKeown, M.R. Hill, M.J. Matthews, *Addit. Manuf.* **2019**, *28*, 228.

Ali Tabatabaeian is a Ph.D. student at the *University of Glasgow*, *United Kingdom*. He completed his M.Sc. degree at the *University of Kashan*, *Iran*, where he did research on the influence of different thermo-mechanical factors on the residual stresses in laminated composite materials. He was awarded as the distinguished researcher of the year and author of the best M.Sc. thesis of the year in university-wide and nationwide completions, respectively. His current research focuses on developing novel bio-inspired smart composites for structural health monitoring applications. His research has led to the publication of more than 20 scientific papers in various international journals and conferences.